Convergence analysis of a class of iterative methods for propagation of reaction fronts in porous media

Loubna Salhi[a], Mohammed Seaid[b], Driss Yakoubi[c,*]

[a]*Laboratory Complex Systems and Interactions, Ecole Centrale of Casablanca, Morocco.*
[b]*Department of Engineering, University of Durham, South Road, Durham DH1 3LE, UK*
[c]*Léonard de Vinci Pôle Universitaire, Research Center, 92 916 Paris La Défense, France*

Abstract

We present an iterative scheme for the numerical analysis of propagating reaction front problems in porous media satisfying an Arrhenius-type law. The governing equations consist of the Darcy equations for the pressure and flow field coupled to two convection–diffusion–reaction equations for the temperature and depth of conversion. Well-posedness, existence and uniqueness of the weak solution are first studied using a fixed-point approach and then, analysis of the proposed iterative scheme is investigated. Numerical results are also presented in order to validate the theoretical estimates and to illustrate the performance of the proposed scheme. The obtained results are in line with our expectations for a good numerical resolution with high accuracy and stability behaviors.

Keywords: Reaction fronts; Darcy flow; Porous media; Iterative scheme; Fixed-point method.

1. Introduction

When the cold reactants are separated from the high-temperature reaction products by a relatively narrow propagation zone in which an exothermic reaction takes place, this zone is known by reaction front. From a modelling point of view, and in case of propagation in a saturated porous medium, many reaction front problems are governed by coupling the convection-diffusion-reaction equations and the Darcy equation, see for instance [6, 30]. Coupling the convection-diffusion equations with the Darcy law has been the subject for several studies, see for instance [9, 15, 36, 35, 39]. The special case of reaction front propagations in porous media occurs in many physical and engineering applications including, combustion modelling and control, chemical reactor industry, insulation of equipment and buildings, nuclear waste disposal and carbon dioxide geological storage among others, see [22, 6, 29, 30, 34]. From a mathematical point of view, the existence and uniqueness of a weak solution for Darcy-convection-diffusion-reaction problems have been presented for example in [9, 17, 21]. Optimal *a priori* error estimates have also been established based on various approaches such as, the Brezzi-Rappaz-Raviart theorem, the modified polynomial projection stabilized technique, see [28, 34, 35]. In the numerical framework, many methods have been presented for solving these problems such as, implicit finite difference schemes, mixed finite element and finite volume methods, spectral discretizations, Raviart-Thomas finite element methods, and semi-Lagrangian methods, see for instance [2, 9, 28, 34, 35]. **A temporal splitting scheme has also been studied in [22] for solving a class of thermal single-phase flows and reactive transport in fractured porous media.** To the best of our knowledge, the well-posedness, the analysis and the efficient numerical approximation of coupled Darcy-convection-diffusion-reaction problems is still a challenging area of research, especially in the case where the viscosity and diffusion coefficients are nonlinear depending on some critical parameters

*Corresponding author

Email addresses: loubna.salhi@centrale-casablanca.ma (Loubna Salhi), m.seaid@durham.ac.uk (Mohammed Seaid), driss.yakoubi@devinci.fr (Driss Yakoubi)

in the governing equations. Note that such problems are strongly coupled so that inaccuracies in one unknown directly influences all other unknowns in the system. In the case of convection-dominated problems, especially when the diffusion coefficients are negligible compared to those of the flow field, convective terms could be a source of instabilities and non-physical oscillations. Moreover, in some chemical reaction problems with very complex interactions and mechanisms, numerical artifacts could be a source of completely illogical and wrong predictions [5]. More often, the governing equations become dominated by the reaction term, especially when it comes to exothermic chemical reactions. In such cases, the numerical solutions tend to give rise to shocks, complex structures, sharp moving fronts and boundary layers, where considerable physical and chemical phenomena occur, see for instance [18, 31, 40].

In the current study, we are interested in the particular case where reaction front problems are satisfying the well-known Arrhenius law [3, 34, 38]. The governing equations consist of coupling the Darcy equations for the pressure and velocity to two convection–diffusion–reaction equations for the temperature and depth of conversion. It should be mentioned that the basis of the Arrhenius law is a principle of physical chemistry which states that the temperature dependence of the reaction rate can be explained by applying the concept of activation energy, see for instance [26, 27]. This concept is present in all kinetic theories, and it explains the exponential nature of the Arrhenius empirical relationship [12]. Similar class of problems has been widely investigated in the literature, see for example [2, 3, 34, 38]. In [3, 38], a linear stability analysis was performed for a model similar to the one investigated in this study. This analysis focuses on the determination of the instability thresholds depending on certain critical parameters such as the Rayleigh number, the Zeldovich number and the Lewis number. Linear stability analysis is often useful when numerical methods become limited in resolution and when it is particularly difficult to use them to find instability thresholds, or to understand the inviscid nature of the instability in numerical models. For these and other technical reasons, it is often necessary to carry out this analysis as a preliminary step before proceeding to the numerical solution. For instance, a convergence analysis of iterative methods for a class of coupled Darcy-convection-diffusion problems has been investigated in [19, 37]. In these references, a fixed-point algorithm is used to study the existence and uniqueness of weak solutions for the considered problems. Numerical results have also been presented in [19, 37] for several problems of natural convection problems in porous media to demonstarte the accuracy and convergence of the iterative schemes. However, the governing equations for the propagation of reaction fronts in porous media considered in this study are more challenging than those coupled Darcy-convection-diffusion problems studied in [19, 37] such that the current problems include two sets of coupled convection-diffusion equations for the temperature and depth of conversion with nonlinear coefficients. Here, the nonlinearity in the present problem is very strong in the sense that nonlinear fluid viscosity and coupled nonlinear reaction terms are accounted for in its modelling. It should be stressed that in contrast to the study carried out in [19, 37], in the current work we seek for the velocity field a more regular space such that the nonlinear terms in equations of temperature and depth of conversion are well defined. In addition, because the spatial domain is assumed to be rectangular, an extension (lifting) of the Dirichlet conditions is explicitly constructed and it is a very regular function. This would simplify the existence and convergence analysis. The aim is to prove well-posedness, existence and uniqueness of the weak solution, and also to establish *a priori* error estimates based on the well-known Brouwer's fixed-point theorem [20, 23]. Next, we present an iterative scheme based on a Picard approach for the numerical solution of the associated fixed point problem. The key idea is to solve at each iteration a linear Darcy equation with the previously computed temperature solution of the preceding iteration. Subsequently, we introduce the known velocity solution in the convection-diffusion-reaction equations with nonlinear coefficients obtained from the previous fixed-point step. In order to evaluate the accuracy of the proposed iterative scheme, we present numerical results for a test problem with known exact solution and also for the benchmark problem of reaction front propagation in porous media. The obtained results are in good agreement with our theoretical expectations and illustrate good numerical behaviors in terms of stability and accuracy.

The rest of the paper is structured as follows: The mathematical formulation of the reaction front problem in porous media is presented in Section 2. Preliminaries, functional spaces and assumptions used are introduced in Section 3. The variational formulation along with *a priori* error estimates are presented in Section 4. The analysis of the proposed iterative scheme is presented in Section 5. Numerical results obtained for two examples of reaction front propagations in porous media are illustrated in Section 6. Conclusions and perspectives are presented in Section 7.

2. Governing equations

Let $\Omega \subset \mathbb{R}^2$ be a two-dimensional bounded domain with Lipschitz continuous boundary $\partial\Omega$. The domain is considered embedded in a saturated porous medium and subject to a thermal variation $(T'_H - T'_C)$, where T'_H and T'_C are temperatures of the hot and cold boundary walls. The thermo-physical properties of the fluid and the medium are assumed to be isotropic and constant except for the fluid viscosity whose variation results mainly from thermal effects, while the thermal conductivity and depth diffusivity depend only on spatial variations. Under the Boussinesq approximation, the change in density, which leads a fluid movement, may be neglected except for the buoyancy force. Under these assumptions, the governing equations are: Darcy equations:

$$\begin{aligned} \epsilon\mu(T')\,\boldsymbol{u}' &= -K_p\left(\nabla p' - \frac{g}{g_c}\beta\rho_0\,(T' - T'_0)\,\boldsymbol{e}\right), && \text{in } \Omega, \\ \nabla\cdot\boldsymbol{u}' &= 0, && \text{in } \Omega, \end{aligned} \tag{1}$$

Energy equation:

$$\rho_0 c_p\,(\boldsymbol{u}'\cdot\nabla T') - \epsilon\nabla\cdot(\lambda'\nabla T') = \mathcal{K}(T',\alpha')Q', \qquad \text{in } \Omega, \tag{2}$$

Depth of conversion equation:

$$\boldsymbol{u}'\cdot\nabla\alpha' - \epsilon\nabla\cdot(\gamma'\nabla\alpha') = \mathcal{K}(T',\alpha'), \qquad \text{in } \Omega, \tag{3}$$

where $\nabla = \left(\dfrac{\partial}{\partial x'}, \dfrac{\partial}{\partial y'}\right)^\top$ denotes the gradient operator. Here, the primed functions and variables refer to dimensional quantities. **In the above equations, $\boldsymbol{u}' = (u', v')^\top$ in $[ms^{-1}]$ is the velocity field, p' in $[Pa]$ is the pressure, T' in $[K]$ is the temperature, α' the depth of conversion, K_p in $[m^2]$ is the permeability, ϵ is the porosity coefficient, $\mu(T')$ in $[kg\ m^{-1}s^{-1}]$ is the dynamic fluid viscosity, g in $[ms^{-2}]$ is the gravity acceleration, β in $[K^{-1}]$ is the coefficient of thermal expansion, ρ_0 in $[kg\ m^{-3}]$ is the reference density, g_c a conversion constant, $\boldsymbol{e}$ the unit vector associated with the gravity, c_p in $[J\ kg^{-1}K^{-1}]$ is the specific heat at constant pressure, λ' in $[W\ m^{-1}K^{-1}]$ is the thermal conductivity coefficient, γ' in $[m^2s^{-1}]$ is the depth diffusivity coefficient, Q' in $[kg\ m^{-1}s^{-2}]$ is the adiabatic heat release. On the boundary, we consider the following conditions**

$$\begin{aligned} &T' = T'_0, \quad \alpha' = 0 \quad \textbf{and} \quad \boldsymbol{u}' = 0, \qquad \textbf{on} \quad \Gamma_{low}, \\ &T' = T'_\infty, \quad \alpha' = 1 \quad \textbf{and} \quad \boldsymbol{u}' = 0, \qquad \textbf{on} \quad \Gamma_{high}. \end{aligned} \tag{4}$$

where T'_0 is the mean temperature and T'_∞ is the ambient temperature, both in $[K]$, the boundary regions Γ_{low} and Γ_{high} are defined as

$$\Gamma_{low} = \left\{\mathbf{x}\in\partial\Omega : \quad \boldsymbol{u}'\cdot\mathbf{n} \geq 0\right\}, \qquad \Gamma_{high} = \left\{\mathbf{x}\in\partial\Omega : \quad \boldsymbol{u}'\cdot\mathbf{n} < 0\right\}.$$

with $\mathbf{n}$ is the unit outward normal vector to the boundary $\partial\Omega$. Notice that in the above and in what follows bold face type denotes vector quantities.

In (2)-(3), the function $\mathcal{K}(T',\alpha') = k(T')\Phi(\alpha')$ describes the reaction rate where the temperature dependence is given by the Arrhenius law [34]

$$k(T') = \epsilon k_0 \exp\left(-\frac{E}{R_0 T'}\right), \tag{5}$$

where k_0 in $[s^{-1}]$ is the pre-exponential factor, R_0 in $[J\ mol^{-1}K^{-1}]$ is the universal gas constant and E in $[J\ mol^{-1}K^{-1}]$ is the activation energy assumed to be very large in the present study. The kinetic function $\Phi_\alpha(\alpha')$ is assumed to be independent of the reactant concentration and defined by the first-order reaction approximation as

$$\Phi_\alpha(\alpha') = 1 - \alpha', \quad 0 \leq \alpha' \leq 1. \tag{6}$$

To reformulate the equations in a dimensionless form, we define the following dimensionless variables and parameters

$$x = \frac{x'c}{\kappa}, \quad y = \frac{y'c}{\kappa}, \quad \boldsymbol{u} = \frac{\boldsymbol{u}'}{\epsilon c}, \quad \mu(T) = \frac{\mu(T')}{\mu_0}, \quad p = \frac{K_p p'}{\epsilon^2 \kappa \mu(T')}, \quad \alpha = \alpha', \quad T = \frac{T' - T'_\infty}{Q}, \tag{7}$$

where μ_0 is a reference dynamic viscosity, the heat release Q and thermal diffusivity κ are defined as

$$Q = \frac{Q'}{\epsilon \rho_0 c_p} = T'_H - T'_C, \qquad \kappa = \frac{\lambda}{\rho_\infty c_p}, \tag{8}$$

and c is the characteristic velocity given by [3, 34]

$$c^2 = \frac{k_0 \kappa R_0 T_\infty^{'2}}{QE} \exp\left(-\frac{E}{R_0 T_\infty^{'2}}\right).$$

We also define the following dimensionless parameters

$$P_r = \frac{\mu}{\kappa}, \qquad R_a = \frac{\beta g Q \kappa^2}{\mu c^3}, \qquad R_p = \frac{K_p c^2 P_r R_a \rho_0}{\epsilon^2 \mu^2 g_c}, \qquad Z = \frac{QE}{R_0 T'^2_\infty}, \qquad L_e = \frac{\kappa}{\gamma}, \tag{9}$$

with

$$\lambda = \frac{\lambda'}{\lambda'_0}, \qquad \gamma = \frac{\gamma'}{\gamma'_0}, \qquad T_0 = \frac{T'_\infty - T'_0}{Q}, \qquad \delta = \frac{R_0 T'_\infty}{E},$$

where P_r, R_a, L_e and Z are the Prandtl number, the Rayleigh number, the Lewis number and the Zeldovich number, respectively. Here, λ'_0 and γ'_0 are reference thermal conductivity and depth diffusivity, respectively. Hence, equations (1)-(4) can be rewritten in a coupled dimensionless form as

$$\begin{aligned} \mu(T)\,\boldsymbol{u} + \nabla p &= \boldsymbol{f}(T), \qquad \text{in } \Omega, \\ \nabla \cdot \boldsymbol{u} &= 0, \qquad \text{in } \Omega, \end{aligned} \tag{10a}$$

for the Darcy problem and

$$\begin{aligned} \boldsymbol{u} \cdot \nabla T - \nabla \cdot (\lambda \nabla T) = \mathcal{K}(T, \alpha), \qquad \text{in } \Omega, \\ \boldsymbol{u} \cdot \nabla \alpha - \nabla \cdot (\gamma \nabla \alpha) = \mathcal{K}(T, \alpha), \qquad \text{in } \Omega, \end{aligned} \tag{10b}$$

for the convection-diffusion equations. Equations (10a)-(10b) are subject to the following boundary conditions

$$\begin{aligned} T = -1, \quad \alpha = 0 \quad \text{and} \quad \boldsymbol{u} = 0, \qquad \text{on} \quad \Gamma_{low}, \\ T = 0, \quad \alpha = 1 \quad \text{and} \quad \boldsymbol{u} = 0, \qquad \text{on} \quad \Gamma_{high}. \end{aligned} \tag{11}$$

It should be stressed that for most free-convective heat and mass transfer applications in porous media, the fluid viscosity $\mu(T)$ is supposed to vary with temperature as

$$\mu(T) = \frac{\mu_\infty}{\big(1 + \nu(T - T_0)\big)}, \tag{12}$$

where μ_∞ and ν are constants whose values depend on the reference state and the thermal properties of the fluid [25]. In equations (10b), the functions $\mathbf{f}$ and $\mathcal{K}$ are defined by

$$\mathbf{f}(T) = R_p\,(T + T_0)\,\boldsymbol{e}, \qquad \mathcal{K}(T,\alpha) = W_Z\,(T)\,\Phi_\alpha(\alpha), \tag{13}$$

where $\Phi_\alpha(\alpha) = 1 - \alpha$ according to (6), and $W_Z\,(T)$ is the dimensionless reaction function defined as

$$W_Z\,(T) = Z \exp\left(\frac{T}{Z^{-1} + \delta T}\right). \tag{14}$$

Notice that the exponent term $-E/R_0T'$ in the Arrhenius formula (5) represents the ratio between the activation energy E and the average kinetic energy R_0T'. For most practical kinetic applications with highly exothermic reactions, the dependence on the temperature is negligible compared to the activation energy *i.e.*, $E >> R_0T'$. Therefore, it becomes apparent with the negative sign in (5) that low rate is obtained for high values of this ratio. This ensures that a high activation energy yields less substantial effects on the exponential term and therefore its variation with temperature becomes very small, see for example [41] for further details. Thus, the dimensionless Arrhenius function (14) can be interpreted as a form of exponential decay law. As a consequence, $\mathcal{K}(T,\alpha)$ in (13) is a bounded continuous real function which can be approximated by a Lipschitz function. **It should also be pointed out that in many applications in front propagation problems (10), the heat is transferred through the fluid in a laminar and stable manner for the considered values of the Rayleigh number R_p and The Zeldovich number Z that are usually low. However, as these values increase, the temperature gradients in the reaction zone become higher, the viscous effects become less important and the buoyancy forces become stronger, so that the convection becomes the more dominant form and the heat transfer becomes increasingly unstable. In the present study, the importance of the choice of assumptions and the values relative to these characteristic parameters lies in the fact that, on the one hand, it respects this physical property of this type of problems, and on the other hand, it complies with their defining physical form. For example, the assumption on Z required for the analysis is consistent with the defining formula of δ in (9) since, the average kinetic energy R_0T always remains lower than the activation energy E.**

3. Preliminaries and assumptions

In this section, we introduce the main notations and assumptions to be used throughout this study. To formulate the problem (10a)-(10b) in a variational form, we introduce the following standard Sobolev spaces, see for instance [1, Chap. III and VII] for more details

$$\begin{aligned} L^2(\Omega) &:= \left\{q:\ \Omega \longrightarrow \mathbb{R}: \qquad \int_\Omega q^2 d\Omega < \infty\right\}, \\ L^2_0(\Omega) &:= \left\{q \in L^2(\Omega): \quad \int_\Omega q\ d\Omega = 0\right\}, \end{aligned}$$

with the norm and inner product in $L^2(\Omega)$ are defined as

$$\|w\|_{L^2(\Omega)} = (w,w)^{\frac{1}{2}}, \qquad \forall\, w \in L^2(\Omega),$$

and

$$(w_1, w_2) = \int_\Omega w_1 w_2\ d\Omega \qquad \forall\, w_1, w_2 \in L^2(\Omega).$$

respectively. We also introduce the following spaces

$$\begin{aligned}
\boldsymbol{H}(\mathrm{div},\Omega) &:= \Big\{\boldsymbol{v}\in \boldsymbol{L}^2(\Omega): \quad \nabla\cdot\boldsymbol{v} \in L^2(\Omega)\Big\},\\
\boldsymbol{H}_0(\mathrm{div},\Omega) &:= \Big\{\boldsymbol{v}\in \boldsymbol{H}(\mathrm{div},\Omega): \quad \boldsymbol{v}\cdot\boldsymbol{n}=0, \quad \text{on } \partial\Omega\Big\},\\
\boldsymbol{V}(\Omega) &:= \Big\{\boldsymbol{v}\in \boldsymbol{H}_0(\mathrm{div},\Omega): \quad \nabla\cdot\boldsymbol{v}=0, \quad \text{in } \Omega\Big\},\\
H^1(\Omega) &:= \Big\{\varphi\in L^2(\Omega): \quad \partial^k\varphi\in L^2(\Omega), \quad \forall\,|k|\le 1\Big\},
\end{aligned}$$

and

$$H^1_{\Gamma_d}(\Omega) := \Big\{\varphi\in H^1(\Omega), \quad \varphi=0 \quad \text{on } \Gamma_d\Big\},$$

where Γ_d is a part of the boundary $\partial\Omega$ with non–negative measure. Let us recall the following Poincaré–Friedrichs inequality

Lemma 3.1. *There exists a non–negative constant C_{PF} which depend only on Ω such that*

$$\|\varphi\| \le C_{PF}\|\nabla\varphi\|, \qquad \forall\varphi\in H^1_{\Gamma_d}(\Omega).$$

Furthermore, if Ω is convex, the Poincaré–Friedrichs constant C_{PF} satisfies

$$C_{PF} \le \frac{d}{\pi}, \tag{15}$$

where d denotes the diameter of Ω defined by

$$d = \sup\left\{\mathrm{distance}\,(\boldsymbol{x},\boldsymbol{y})\,; \qquad (\boldsymbol{x},\boldsymbol{y})\in\Omega\right\}.$$

In the present study, the spatial domain Ω is assumed to be rectangular $\Omega =]0,1[\times]-L,L[$, with $L>0$ and we denote by Γ_d its boundary parts defined by

$$\Gamma_d = \Big\{(x,y); \quad 0\le x\le 1; \quad y=\pm L\Big\}, \qquad \Gamma_n = \partial\Omega\setminus\Gamma_d.$$

Note that this assumption is used here for simplicity in the presentation only, but the analysis presented in this study is still applicable for general rectangular domains. Hence, using the assumption on the spatial domain, the inequality (15) becomes

$$C_{PF} \le \frac{\sqrt{\mathbf{L^2+1}}}{\pi}. \tag{16}$$

On the other hand, the boundary conditions can be rewritten as follow

$$\begin{aligned}
T=-1, \quad \alpha=0 \quad \text{and} \quad u=0, \quad \text{on} \quad y=L,\\
T=0, \quad \alpha=1 \quad \text{and} \quad u=0, \quad \text{on} \quad y=-L.
\end{aligned} \tag{17}$$

In addition, we also assume that

$$\delta Z < 1. \tag{18}$$

Then, under (18), we get

$$W_m := Z\exp\left(\frac{Z}{1-\delta Z}\right) \le W_Z(T) \le Z\exp\left(\frac{1}{Z}\right) := W_M, \qquad \forall\, T\ge -1. \tag{19}$$

In addition, we consider the following assumptions

Hypothesis 3.2. *The functions μ, λ and γ are assumed to be:*

(H1) μ is Lipschitz–continuous function with Lipschitz constant L_μ: for all ℓ, $s \in \mathbb{R}$ with

$$|\mu(\ell) - \mu(s)| \leq L_\mu |\ell - s|$$

(H2) bounded from above and from below by positive constants μ_i, λ_i and γ_i, $i = 1, 2$ for all $\ell \in \mathbb{R}$ and for all $\boldsymbol{x} \in \Omega$ as

$$\mu_1 \leq \mu(\ell) \leq \mu_2, \qquad \lambda_1 \leq \lambda(\boldsymbol{x}) \leq \lambda_2 \qquad \textit{and} \qquad \gamma_1 \leq \gamma(\boldsymbol{x}) \leq \gamma_2.$$

For any real function β, we denote by β^+ and β^- the following functions

$$\beta^+ := \max(\beta, 0) \text{ and } \beta^- := \min(\beta, 0).$$

It should be noted that the above assumptions related to certain characteristic parameters are acceptable from a physical view as long as they respect their definitional forms. For instance, in Assumption (18), if expressions for δ and Z defined in (9) are considered, then δZ takes the form $\delta\, Z = \frac{Q}{T'_\infty}$, with T'_∞ is the highest ambient temperature reached during the exothermic reaction. This temperature relative to the heat release Q defined in (8) always remains higher, leading to a form of δZ that always remains lower than 1. Needless to mentiona that the considered assumptions are necessary for the analysis study of the existence and uniqueness for the solution of the coupled problem (10a)-(10b).

4. Analysis of the variational formulation

The variational formulation of the coupling problem (10) can be written as follow: Find $(\boldsymbol{u}, p) \in \boldsymbol{L}^3(\Omega) \cap \boldsymbol{V}(\Omega) \times (H^1(\Omega) \cap L^2_0(\Omega))$ and $(T, \alpha) \in H^1(\Omega) \times H^1(\Omega)$ such that (17) holds and that

$$\int_\Omega \mu(T)\boldsymbol{u} \cdot \boldsymbol{v}\, d\Omega + \int_\Omega \boldsymbol{v} \cdot \nabla p\, d\Omega = \int_\Omega \boldsymbol{f}(T) \cdot \boldsymbol{v}\, d\Omega, \qquad \forall \boldsymbol{v} \in \boldsymbol{L}^2(\Omega), \tag{20}$$

$$\int_\Omega \boldsymbol{u} \cdot \nabla q\, d\Omega = 0, \qquad \forall q \in H^1(\Omega) \cap L^2_0(\Omega), \tag{21}$$

$$\int_\Omega \boldsymbol{u} \cdot \nabla T\, \varphi\, d\Omega + \int_\Omega \lambda(\boldsymbol{x})\nabla T \cdot \nabla\varphi\, d\Omega = \int_\Omega W_Z(T)\Phi_\alpha(\alpha)\, \varphi\, d\Omega, \qquad \forall \varphi \in H^1_{\Gamma_d}(\Omega), \tag{22}$$

$$\int_\Omega \boldsymbol{u} \cdot \nabla\alpha\, \eta\, d\Omega + \int_\Omega \gamma(\boldsymbol{x})\nabla\alpha \cdot \nabla\eta\, d\Omega = \int_\Omega W_Z(T)\Phi_\alpha(\alpha)\, \eta\, d\Omega, \qquad \forall \eta \in H^1_{\Gamma_d}(\Omega). \tag{23}$$

Since the space $\mathcal{D}(\Omega \cup \Gamma_n)$ **(defined as the set of functions in $C^\infty(\Omega \cup \Gamma_n)$ which are compactly supported in $\Omega \cup \Gamma_n$)** is dense in $H^1_{\Gamma_d}(\Omega)$ (see for instance [8, 14]) the variational formulation (20)-(23) is equivalent to the coupled problem (10) (in the sense of distribution), see for example [9].

Thanks to the following inf–sup condition [4]

$$\forall q \in H^1(\Omega), \qquad \sup_{\boldsymbol{v} \in \boldsymbol{L}^2(\Omega)} \frac{\int_\Omega \boldsymbol{v} \cdot \nabla q}{\|\boldsymbol{v}\|} \leq \|\nabla q\|. \tag{24}$$

Then, the variational Darcy problem (20)-(21) is equivalent to find $\boldsymbol{u} \in \boldsymbol{V}(\Omega)$ solution of

$$\int_\Omega \mu(T)\boldsymbol{u} \cdot \boldsymbol{v}\, d\Omega = \int_\Omega \boldsymbol{f}(T) \cdot \boldsymbol{v}\, d\Omega, \qquad \forall \boldsymbol{v} \in \boldsymbol{V}(\Omega). \tag{25}$$

Therefore $(\boldsymbol{u}, T, \alpha) \in \boldsymbol{L}^3(\Omega) \cap \boldsymbol{V}(\Omega) \times H^1(\Omega) \times H^1(\Omega)$ is the solution of (25)-(22)-(23).

We introduce the following functions and notations to establish all estimates in H^1-norms. We set the functions $\bar{\alpha}$ and $\bar{T}$ defined as

$$\bar{\alpha}(x,y) := \frac{2}{L^2}y(y-L) \qquad \bar{T}(x,y) := \frac{2}{L^2}y(y+L). \tag{26}$$

It is clear that

$$r_0^2 := \|\bar{\alpha}\|^2 = \|\bar{T}\|^2 = \frac{64\,L}{15}, \qquad r_1^2 := \|\nabla\bar{\alpha}\|^2 = \|\nabla\bar{T}\|^2 = \frac{56}{3\,L}, \quad \text{and} \quad \|\bar{\alpha}\|_{L^\infty} = \|\bar{T}\|_{L^\infty} = \frac{1}{2}. \tag{27}$$

Let us also introduce these constants

$$\kappa_1 = \frac{\gamma_2^2 r_1^2}{2\gamma_1^2} + \frac{2LW_M}{\gamma_1} \qquad \kappa_2 = \frac{W_M L r_1}{\lambda_1 \pi} + \frac{W_M^2 L^2}{\lambda_1^2 \pi^2}. \qquad \kappa_\star = 1 - \frac{2R_p^2 L^2}{\lambda_1^2 \mu_1^2 \pi^2}. \tag{28}$$

Lemma 4.1. *Assume that Hypothesis 3.2 holds. For any solution* $(\boldsymbol{u}, T, \alpha) \in \boldsymbol{L}^3(\Omega) \cap \boldsymbol{V}(\Omega) \times H^1(\Omega) \times H^1(\Omega)$ *of problem* (25)-(22)-(23)*, the followings estimates hold*

$$-1 \leq T(\boldsymbol{x}) \ \ \textit{and} \ \ 0 \leq \alpha(\boldsymbol{x}) \leq 1, \qquad \textit{a.e}\ \boldsymbol{x} \ \ \textit{in} \ \ \Omega \tag{29}$$

Furthermore, if

$$\frac{R_p}{\mu_1} < \frac{\pi}{\sqrt{2}\,L}\lambda_1, \tag{30}$$

then

$$\begin{aligned}
\|\nabla T\| &\leq M_T := \left(\frac{2R_p^2}{\kappa_\star}\|T_0\|^2 + \frac{\kappa_2}{\kappa_\star}\right)^{\frac{1}{2}}, &(31)\\
\|\boldsymbol{u}\| &\leq M_u := \frac{R_p}{\mu_1}\left(\|T_0\| + \frac{\sqrt{\mathbf{L^2+1}}}{\pi}M_T\right), &(32)\\
\|\nabla\alpha\| &\leq M_\alpha := \left(\frac{M_u^2}{2\mu_1^2} + \kappa_1\right)^{\frac{1}{2}}. &(33)
\end{aligned}$$

Proof. We start by showing that the solution of (23) satisfies

$$0 \leq \alpha(\boldsymbol{x}) \leq 1, \quad a.e \text{ in } \Omega.$$

Thus, taking $\eta = \alpha^-$ which is an element of $H^1_{\Gamma_d}(\Omega)$ and using the definition of Φ_α, we obtain

$$\begin{aligned}
\int_\Omega W_Z(T)\,\alpha^-\,d\Omega &= \int_\Omega W_Z(T)\,\alpha\,\alpha^-\,d\Omega + \int_\Omega \boldsymbol{u}\cdot\nabla\alpha\,\alpha^-\,d\Omega + \int_\Omega \gamma(\boldsymbol{x})\nabla\alpha\cdot\nabla\alpha^-\,d\Omega,\\
&= \int_\Omega W_Z(T)\,|\alpha^-|^2\,d\Omega + \int_\Omega \boldsymbol{u}\cdot\nabla\alpha^-\,\alpha^-\,d\Omega + \int_\Omega \gamma(\boldsymbol{x})\,|\nabla\alpha^-|^2\,d\Omega.
\end{aligned}$$

Since $W_Z(\cdot)$ is non–negative and $\nabla\cdot\boldsymbol{u} = 0$ in Ω, we deduce that

$$\int_\Omega W_Z(T)\,|\alpha^-|^2\,d\Omega + \int_\Omega \gamma(\boldsymbol{x})\,|\nabla\alpha^-|^2\,d\Omega = 0.$$

Hence, $\alpha^- = 0 \quad a.e$ in Ω and thus $\alpha \geq 0,\ a.e$ in Ω.

Next, taking $\eta = (\alpha-1)^+$ which belongs to $H^1_{\Gamma_d}(\Omega)$ in (23), we obtain

$$\int_\Omega \boldsymbol{u}\cdot\nabla\alpha\,(\alpha-1)^+\,d\Omega + \int_\Omega \gamma(\boldsymbol{x})\nabla\alpha\cdot\nabla(\alpha-1)^+\,d\Omega = \int_\Omega W_Z(T)\,(1-\alpha)(\alpha-1)^+\,d\Omega.$$

Then,

$$\int_\Omega \boldsymbol{u}\cdot\nabla((\alpha-1)^+)\,(\alpha-1)^+\,d\Omega+\int_\Omega \gamma(\boldsymbol{x})|\nabla(\alpha-1)^+|^2\,d\Omega=-\int_\Omega W_Z(T)\,|(\alpha-1)^+|^2\,d\Omega.$$

According to the incompressibility condition, the first term in the left-hand side vanishes. Since the second term is negative, we have

$$\gamma_1\|\nabla((\alpha-1)^+)\|^2\ \le\ \int_\Omega \gamma(\boldsymbol{x})|\nabla(\alpha-1)^+|^2\,d\Omega=0.$$

Thanks to the Poincaré–Friedrichs inequality, we deduce that $(\alpha-1)^+=0,\ a.e$ in Ω, which is equivalent to $\alpha\le 1,\ a.e\,\Omega$.

Concerning the temperature, for $\varphi=(T+1)^-\in H^1_{\Gamma_d}(\Omega)$ in (22), using the previous arguments and $0\le W_Z(T)\Phi_\alpha(\alpha)$, $a.e$ in Ω, yields

$$\lambda_1\|\nabla((T+1)^-)\|^2\le 0.$$

Once again the Poincaré–Friedrichs inequality yields $T\ge -1$, $a.e$ in Ω, which complete the proof of (29).

By construction (27), it is clear that both functions $\eta:=\alpha-\bar\alpha$ and $\varphi:=\bar T-T$ belong to $H^1_{\Gamma_d}(\Omega)$. Then, taking $\eta:=\alpha-\bar\alpha$ as a test function in (23), one obtains

$$\int_\Omega \boldsymbol{u}\cdot\nabla\alpha\,\alpha+\int_\Omega\gamma(\boldsymbol{x})|\nabla\alpha|^2+\int_\Omega W_Z(T)\alpha^2=\int_\Omega \boldsymbol{u}\cdot\nabla\alpha\,\bar\alpha+\int_\Omega\gamma(\boldsymbol{x})\nabla\alpha\cdot\nabla\bar\alpha+\int_\Omega W_Z(T)\,(\alpha-\bar\alpha+\alpha\bar\alpha)\,.$$

According to the incompressibility of the velocity, the first term in the left-hand side vanishes. Thanks to assumption 3.2, (19), (27) and the Cauchy-Schwarz inequality, we obtain

$$\begin{aligned}\gamma_1\|\nabla\alpha\|^2+W_m\|\alpha\|^2 &\le \|\boldsymbol{u}\|\|\bar\alpha\|_{L^\infty}\,\|\nabla\alpha\|\|\,+\gamma_2\|\nabla\alpha\|\|\nabla\bar\alpha\|\,+\,2LW_M\Big(\|\bar\alpha\|_{L^\infty}+\|\alpha\|_{L^\infty}+\|\bar\alpha\|_{L^\infty}\|\alpha\|_{L^\infty}\Big),\\ &\le\frac12\|\boldsymbol{u}\|\,\|\nabla\alpha\|\|\,+\gamma_2 r_1\|\nabla\alpha\|+4LW_M.\end{aligned}$$

The Young's inequality gives

$$\gamma_1\|\nabla\alpha\|^2\le\frac{1}{4\gamma_1}\,\|\boldsymbol{u}\|^2\,+\frac{\gamma_2^2r_1^2}{4\gamma_1}\,+\,4LW_M+\frac{\gamma_1}{2}\|\nabla\alpha\|^2.$$

Finally,

$$\|\nabla\alpha\|^2\le\frac{1}{2\gamma_1^2}\|\boldsymbol{u}\|^2+\kappa_1, \tag{34}$$

To bound T in H^1-norm, let $\varphi=T-\bar T$ in (22) which is an admissible test function. Applying same techniques as before, we obtain

$$\lambda_1\|\nabla T\|^2\le W_M\|1-\alpha\|\,\|T-\bar T\|+\|\boldsymbol{u}\|\|\nabla T\|\|\bar T\|_{L^\infty}+\lambda_2\|\nabla T\|\,\|\nabla\bar T\|.$$

Using successively **the Poincaré–Friedrichs** inequality, the Young's inequality, (29), (27) and (29) we obtain

$$\begin{aligned}\lambda_1\|\nabla T\|^2&\le W_M\|1-\alpha\|\,\|T-\bar T\|+\|\boldsymbol{u}\|\|\nabla T\|\|\bar T\|_{L^\infty}+\lambda_2\|\nabla T\|\,\|\nabla\bar T\|,\\&\le 2W_MC_{PF}\left(\|\nabla T\|+\|\nabla\bar T)\|\right)+\frac12\|\boldsymbol{u}\|\|\nabla T\|+\lambda_2\|\nabla T\|\,\|\nabla\bar T\|,\\&\le 2r_1W_MC_{PF}+2W_MC_{PF}\|\nabla T\|+\frac{r_1}{2}\|\boldsymbol{u}\|+\frac12\|\boldsymbol{u}\|\|\nabla T\|,\\&\le 2W_MC_{PF}r_1+\frac{W_M^2C_{PF}^2}{4\lambda_1}+\frac{1}{8\lambda_1}\|\boldsymbol{u}\|^2+\frac{\lambda_1}{2}\|\nabla T\|^2.\end{aligned}$$

Then,

$$\|\nabla T\|^2 \leq \frac{1}{4\lambda_1^2}\|\boldsymbol{u}\|^2 + \kappa_2. \tag{35}$$

On the other hand, we take $\boldsymbol{v} = \boldsymbol{u}$ in Darcy equation, we get (25)

$$\mu_1\|\boldsymbol{u}\| \leq R_p\left(\|T\| + \|T_0\|\right).$$

Thus, we use (35) and the Poincaré–Friedrichs inequality to obtain

$$\|\nabla T\|^2 \leq \frac{R_p^2 C_{PF}^2}{2\lambda_1^2\mu_1^2}\|\nabla T\|^2 + 2R_p^2\|T_0\|^2 + \kappa_2.$$

We deduce the inequality (31) using (16) and the assumption (30). As a result, we proof the estimate (32) and (33). □

Our next concern is the following well–posedness result:

Lemma 4.2. *Assume that Hypothesis 3.2–(H2) holds. For any $T \in L^2(\Omega)$, there exists a unique pair $(\boldsymbol{u}, p) \in \boldsymbol{L}^2(\Omega) \times H^1(\Omega)$ solution of (20)-(21).*

Moreover, if T belongs to $H^1(\Omega)$. Then, for all non–negative real numbers s, with $2 \leq s < +\infty$,

$$(\boldsymbol{u}, p) \ \in \ \boldsymbol{L}^s(\Omega) \times W^{1,s}(\Omega),$$

and the following estimate holds

$$\|\boldsymbol{u}\|_{\boldsymbol{H}^1} \leq C\|T - T_0\|_{H^1}, \tag{36}$$

where the non–negative constant depends only on μ, Ω, s and R_p.

Proof. We refer the reader to [10] (see Theorem 1.9, Chapter XIII) for the existence and uniqueness of the solution $(\boldsymbol{u}, p)$ in $\boldsymbol{L}^2(\Omega) \times H^1(\Omega)$. Next, if the temperature T belongs to $H^1(\Omega)$ and in the case of variable viscosity but not depending on T, we refer to [9] for the regularity of the velocity in $H^1(\Omega)$ and estimate (36).

Now, when μ depends on T, we follow ideas reported in [7] (See Chapter IV). **Hence, we apply the divergence operator to equation (10a), to obtain**

$$\nabla \cdot \left(\frac{1}{\mu(T)}\nabla p\right) = \nabla \cdot \left(\frac{1}{\mu(T)}(T - T_0)\right). \tag{37}$$

Since $T \in H^1(\Omega)$ and the Sobolev injection in dimension $d = 2$, we have $T \in L^s(\Omega)$ for all s, $2 \leq s < +\infty$. Hypothesis 3.2 infers that $\dfrac{1}{\mu(T)}(T - T_0)$ belongs to $L^s(\Omega)$. Then, there exists a unique solution p of (37) such that $p \in H^1(\Omega) \cap L_0^2(\Omega)$ and $\dfrac{1}{\mu(T)}\nabla p \in \boldsymbol{L}^s(\Omega)$. Furthermore, there exists a constant $C > 0$ depends on s, Ω and R_p such that

$$\left\|\frac{1}{\mu(T)}\nabla p\right\|_{\boldsymbol{L}^s} \leq C\left\|\frac{1}{\mu(T)}(T - T_0)\right\|_{L^s}.$$

Finally, back to the Darcy equation (10a), we have using the Sobolev injection from $H^1(\Omega)$ into $L^s(\Omega)$

$$\|\boldsymbol{u}\|_{\boldsymbol{L}^s} \leq C\|T - T_0\|_{L^s} \leq C'\|T - T_0\|_{H^1}.$$

□

Lemma 4.3. *Assume that Hypothesis 3.2–(H2) holds. For any divergence–free function $\boldsymbol{u} \in \boldsymbol{L}^2(\Omega)$ and any function $\alpha \in L^\infty(\Omega)$ such that $0 \leq \alpha(x) \leq 1$, a.e in Ω, the problem (22) admits a unique solution $T \in H^1(\Omega)$.*

Proof. The proof is based on the Schauder fixed point theorem. To this end, let the mapping

$$\begin{aligned}\mathcal{L} : L^2(\Omega) &\mapsto L^2(\Omega),\\ T &\mapsto \mathcal{L}(T) = \theta \in H^1_{\Gamma_d}(\Omega),\end{aligned}$$

which is the unique solution of the following formulation: $\forall \varphi \in H^1_{\Gamma_d}(\Omega)$

$$\begin{aligned}\int_\Omega \boldsymbol{u} \cdot \nabla\theta\, \varphi\, d\Omega + \int_\Omega \lambda(\boldsymbol{x})\nabla\theta \cdot \nabla\varphi\, d\Omega \;\; &= \;\; \int_\Omega W_Z(T)\Phi_\alpha(\alpha)\varphi\, d\Omega - \\ &\int_\Omega \boldsymbol{u} \cdot \nabla\bar{T}\, \varphi\, d\Omega - \int_\Omega \lambda(\boldsymbol{x})\nabla\bar{T} \cdot \nabla\varphi\, d\Omega. \qquad (38)\end{aligned}$$

Since $\|W_Z(T)\Phi(\alpha)\| \le Z\exp(\frac{1}{\delta})\, \|\Phi_\alpha(\alpha))\|$, Hypothesis 3.2$-(H2)$ and the incompressibility condition on $\boldsymbol{u}$, the existence and uniqueness of θ is a direct consequence of the Lax–Milgram theorem [13]. Next, taking $\varphi = \theta$ in (38) and using $-\int_\Omega \boldsymbol{u} \cdot \nabla\bar{T}\, \theta\, d\Omega = \int_\Omega \boldsymbol{u} \cdot \nabla\theta\, \bar{T}\; d\Omega$, the Cauchy-Schwarz inequality combined with (31), gives

$$\lambda_1\|\nabla\theta\|^2 \le W_M\, \|\Phi_\alpha(\alpha)\|\|\theta\| + \|\boldsymbol{u}\|\, \|\nabla\theta\|\|\bar{T}\|_{L^\infty} + \lambda_2\, \|\nabla\theta\|\, \|\nabla\bar{T}\|.$$

We deduce from the Poincaré–Friedrichs inequality and (27) that

$$\|\nabla\theta\| \le \frac{2LW_M}{\pi\lambda_1} + \frac{1}{2\lambda_1}\|\boldsymbol{u}\| + \frac{\lambda_2 r_1}{\lambda_1} \;:= R.$$

Then, $\mathcal{L} :\, L^2(\Omega) \mapsto\; K := \{\varphi \in H^1_{\Gamma_d}(\Omega),\; \|\nabla\varphi\| \le R\}$. It is clear that the set K is convex and thanks to the Rellich theorem, K is compact in $L^2(\Omega)$.

Now, let us prove that the mapping $\mathcal{L} :\; L^2(\Omega) \;\mapsto\; L^2(\Omega)$ is continuous. To this end, we consider a sequence $(T_n)_n \subset L^2(\Omega)$ such that $T_n \to T$ in $L^2(\Omega)$. Since the sequence $\theta_n := \mathcal{L}(T_n)$ belongs to $H^1_{\Gamma_d}(\Omega)$ and it is uniformly bounded ($\|\nabla\theta_n\| \le R$), there exists a subsequence, still denoted by $(\theta_n)_n$ for simplicity, which weakly converges to θ in $H^1_{\Gamma_d}(\Omega)$ and strongly in $L^2(\Omega)$, *a.e* in Ω. On the other hand, the function $\ell \mapsto W_Z(\ell)$ is continuous on $[-1, +\infty[$, then $\lim\limits_{n\to+\infty} W_Z(T_n)\Phi_\alpha(\alpha) = W_Z(T)\Phi_\alpha(\alpha)$ *a.e* in Ω and $|W_Z(T_n)\Phi_\alpha(\alpha)| \le W_M\Phi_\alpha(\alpha)$ *a.e* in Ω. Using the Lebesgue dominated convergence (see, for instance [13]), we have the strong convergence

$$W_Z(T_n)\Phi_\alpha(\alpha) \;\longrightarrow\; W_Z(T)\Phi_\alpha(\alpha), \qquad \text{in } \; L^2.$$

We finally deduce that when n tends to $+\infty$

$$\int_\Omega \boldsymbol{u} \cdot \nabla\theta_n\, \varphi\, d\Omega + \int_\Omega \lambda(\boldsymbol{x})\nabla\theta_n \cdot \nabla\varphi\, d\Omega = \int_\Omega W_Z(T_n)\Phi_\alpha(\alpha)\varphi\, d\Omega - \int_\Omega \boldsymbol{u} \cdot \nabla\bar{T}\, \varphi\, d\Omega - \int_\Omega \lambda(\boldsymbol{x})\nabla\bar{T} \cdot \nabla\varphi\, d\Omega,$$

converges to

$$\int_\Omega \boldsymbol{u} \cdot \nabla\theta\, \varphi\, d\Omega + \int_\Omega \lambda(\boldsymbol{x})\nabla\theta \cdot \nabla\varphi\, d\Omega = \int_\Omega W_Z(T)\Phi_\alpha(\alpha)\varphi\, d\Omega - \int_\Omega \boldsymbol{u} \cdot \nabla\bar{T}\, \varphi\, d\Omega - \int_\Omega \lambda(\boldsymbol{x})\nabla\bar{T} \cdot \nabla\varphi\, d\Omega,$$

which implies that $\theta = \mathcal{L}(T)$. Thanks to the uniqueness of the solution of problem (38), we deduce that the whole sequence $\mathcal{L}(T_n)$ converges to $\mathcal{L}(T)$ in $L^2(\Omega)$. As a direct consequence, the application $\mathcal{L}$ maps the convex $K \subset L^2(\Omega)$ into itself and it is continuous. From Schauder theorem, there exists $T \in K$ such that $\mathcal{L}(T) = T$. Then, the problem (22) admits a unique solution in $H^1(\Omega)$. □

Concerning the problem (23), since the solution α belongs to $[0, 1]$, *a.e* in Ω, the integral $\int_\Omega \boldsymbol{u} \cdot \nabla\alpha\, \eta\, d\Omega$ is well defined for all divergence–free function $\boldsymbol{u} \in L^2(\Omega)$. Furthermore, the function $W_Z(\cdot)$ is bounded uniformly by W_M. Therefore, same arguments used in the proof of Lemma 4.3 can be used to prove the following lemma, then we skip it.

Lemma 4.4. *Assume that Hypothesis 3.2–(H2) holds. For any divergence–free function* $\boldsymbol{u} \in \boldsymbol{L}^2(\Omega)$ *and any function* $T \in L^2(\Omega)$*, the problem* (23) *admits a unique solution* $\alpha \in H^1(\Omega) \cap L^\infty(\Omega)$.

Theorem 4.5. *We assume that Hypothesis 3.2 holds. In addition, if*

$$\delta \geq \frac{1}{2}, \qquad Z \leq \frac{2\delta - 1}{2\delta^2}, \tag{39}$$

and

$$K := \left(\frac{M_T^2 C_S^2}{\lambda_1 \mu_1^2} + \frac{C}{\gamma_1 \mu_1^2} \right) (R_p + L_\mu M_T')^2 \left[\lambda_1 - \frac{8L^2}{\pi^2} \left(|W_Z'(-1)|^2 + \frac{L^2 \left(|W_Z'(-1)|^2 + W_M^2 \right))}{\pi^2 \gamma_1} \right) \right]^{-1} < 1, \tag{40}$$

then, the problem (20)-(23) *admits a unique solution* $(\boldsymbol{u}, p, T, \alpha)$ *in* $\boldsymbol{L}^3(\Omega) \times (H^1(\Omega) \cap L_0^2(\Omega)) \times H^1(\Omega) \times H^1(\Omega)$, *where*

$$M_T' = (1 + C_{PF})\, M_T. \tag{41}$$

Proof. We use the fixed point of Banach theorem to establish this result. Thus, let the mapping $\mathcal{F}_1 : (T, \alpha) \mapsto \boldsymbol{u}$, such that $\boldsymbol{u}$ is the solution of (20)-(21). Thanks to Lemma 4.2, this mapping is well defined and continuous from $H^1(\Omega) \times H^1(\Omega)$ to $\boldsymbol{L}^3(\Omega)$. Now, let the mapping $\mathcal{F}_2$ defined from $\boldsymbol{L}^3(\Omega)$ to $H^1(\Omega) \times H^1(\Omega)$, which associates with any $\boldsymbol{u} \in \boldsymbol{L}^3(\Omega)$ the solution (T, α) of problems (23)-(22). In order to apply the fixed point of Banach theorem to the mapping $\mathcal{F} := \mathcal{F}_2 \circ \mathcal{F}_1$ defined from $H^1(\Omega) \times H^1(\Omega)$ into itself, we must prove that $\mathcal{F}$ is a Lipschitz mapping with the Lipschitz constant $\mathcal{K} < 1$. To this end, let $(T_1, T_2, \alpha_1, \alpha_2)$ and $\left(\hat{T}_1, \hat{T}_2, \hat{\alpha}_1, \hat{\alpha}_2\right)$ in $H^1(\Omega)$ and $\boldsymbol{u}_1, \boldsymbol{u}_2$ in $\boldsymbol{L}^3(\Omega)$ such that

$$\mathcal{F}_1((T_1, \alpha_1)) = \boldsymbol{u}_1, \qquad \mathcal{F}_1((T_2, \alpha_2)) = \boldsymbol{u}_2,$$

$$\mathcal{F}_2(\boldsymbol{u}_1) = (\hat{T}_1, \hat{\alpha}_1), \qquad \mathcal{F}_2(\boldsymbol{u}_2) = (\hat{T}_2, \hat{\alpha}_2).$$

First, taking $\boldsymbol{v} = \boldsymbol{u}_1 - \boldsymbol{u}_2$ in (20), we obtain

$$\int_\Omega \mu(T_1) |\boldsymbol{u}_1 - \boldsymbol{u}_2|^2 \, d\Omega + \int_\Omega (\mu(T_1) - \mu(T_2))\, \boldsymbol{u}_1 \cdot (\boldsymbol{u}_1 - \boldsymbol{u}_2)\, d\Omega = R_P \int_\Omega (T_1 - T_2) \boldsymbol{e} \cdot (\boldsymbol{u}_1 - \boldsymbol{u}_2)\, d\Omega.$$

Hypothesis 3.2, Cauchy-Schwarz inequality and Lemma 4.2 infer that

$$\mu_1 \|\boldsymbol{u}_1 - \boldsymbol{u}_2\|^2 \leq L_\mu \|T_1 - T_2\|_{L^6} \|\boldsymbol{u}_1\|_{\boldsymbol{L}^3} \|\boldsymbol{u}_1 - \boldsymbol{u}_2\| + R_P \|T_1 - T_2\| \, \|\boldsymbol{u}_1 - \boldsymbol{u}_2\|.$$

Thanks to (36) and the Sobolev injection form $H^1(\Omega)$ into $L^6(\Omega)$ and the Poincaré–Friedrichs inequality, we obtain

$$\mu_1 \|\boldsymbol{u}_1 - \boldsymbol{u}_2\| \leq C\, (L_\mu + R_p)\, \|\nabla (T_1 - T_2)\|, \tag{42}$$

On the other hand, the pair $(\mathbf{U}, P)$ such that $\mathbf{U} = \boldsymbol{u}_1 - \boldsymbol{u}_2$ and $P = p_1 - p_2$ satisfies the following Darcy equations

$$\begin{aligned} \mathbf{U} + \frac{1}{\mu(T_1)} \nabla P &= \mathsf{F} := \frac{R_p}{\mu(T_1)} (T_1 - T_2) \boldsymbol{e} + \frac{\mu(T_1) - \mu(T_2)}{\mu(T_1)}\, \boldsymbol{u}_1, \\ \nabla \cdot \mathbf{U} &= 0. \end{aligned} \tag{43}$$

Thanks to Lemma 4.2 and Hypothesis 3.2, the second term F belongs to $L^s(\Omega)$ for all $2 \leq s < +\infty$. Then $(\mathbf{U}, P) \in \boldsymbol{L}^s(\Omega) \times W^{1,s}(\Omega)$ and

$$\|\mathbf{U}\|_{\boldsymbol{L}^s} \leq C \|\mathsf{F}\|_{\boldsymbol{L}^s}, \quad \forall s \in [2, +\infty[,$$

in particular for $s = 3$. Thus using Cauchy-Schwarz inequality, it yields

$$\begin{aligned}\|\mathbf{U}\|_{\boldsymbol{L}^3} &\le \frac{CR_p}{\mu_1}\|T_1 - T_2\|_{L^3} + \frac{L_\mu}{\mu_1}\|(T_1 - T_2)\boldsymbol{u}_1\|_{\boldsymbol{L}^3},\\ &\le \frac{CR_p}{\mu_1}\|T_1 - T_2\|_{L^3} + \frac{L_\mu}{\mu_1}\|T_1 - T_2\|_{L^6}\,\|\boldsymbol{u}_1\|_{\boldsymbol{L}^6}.\end{aligned}$$

Once again, thanks to (36) and the Sobolev injection $H^1(\Omega)$ into $L^6(\Omega)$, we deduce that

$$\|\mathbf{U}\|_{\boldsymbol{L}^3} \le \frac{C}{\mu_1}\|\nabla(T_1 - T_2)\|\,(R_p + L_\mu\|T_1\|_{H^1})\,\|\nabla(T_1 - T_2)\|.$$

From (31), we conclude

$$\|\boldsymbol{u}_1 - \boldsymbol{u}_2\|_{\boldsymbol{L}^3} \le \frac{C}{\mu_1}\,(R_p + L_\mu M'_T)\,\|\nabla(T_1 - T_2)\|, \tag{44}$$

Next, taking $\varphi = \hat{T}_1 - \hat{T}_2$ and $\eta = \hat{\alpha}_1 - \hat{\alpha}_2$ as test functions in (22) and (23), respectively. Adding the two obtained equations and according to the incompressibility condition on the velocity, we have

$$\begin{aligned}\lambda_1\|\nabla(\hat{T}_1 - \hat{T}_2)\|^2 + \gamma_1\|\nabla(\hat{\alpha}_1 - \hat{\alpha}_2)\|^2 + W_Z(-1)\|\hat{\alpha}_1 - \hat{\alpha}_2\|^2 \le \left|\int_\Omega (\boldsymbol{u}_1 - \boldsymbol{u}_2)\nabla\cdot\hat{T}_1\,(\hat{T}_1 - \hat{T}_2)\right| +\\ \left|\int_\Omega (\boldsymbol{u}_1 - \boldsymbol{u}_2)\nabla\cdot\hat{\alpha}_1\,(\hat{\alpha}_1 - \hat{\alpha}2)\right|\left|\int_\Omega (W_Z(\hat{T}_1) - W_Z(\hat{T}_2))(1 - \hat{\alpha}_1)\Big((\hat{T}_1 - \hat{T}_2) + (\hat{\alpha}_1 - \hat{\alpha}_2)\Big)\right| +\\ \left|\int_\Omega W_Z(\hat{T}_2)(\hat{\alpha}_2 - \hat{\alpha}_1)(\hat{T}_1 - T_2)\right|.\end{aligned} \tag{45}$$

From Lemma 4.1 and Lemma 4.2, Hypothesis 3.2 and Cauchy–Schwarz inequality we obtain

$$\begin{aligned}&\lambda_1\|\nabla(\hat{T}_1 - \hat{T}_2)\|^2 + \gamma_1\|\nabla(\hat{\alpha}_1 - \hat{\alpha}_2)\|^2 + W_Z(-1)\|\hat{\alpha}_1 - \hat{\alpha}_2\|^2 \le\\ &\quad M_T\|\boldsymbol{u}_1 - \boldsymbol{u}_2\|_{\boldsymbol{L}^3}\|\hat{T}_1 - \hat{T}_2\|_{L^6} + \|W_Z(\hat{T}_1) - W_Z(\hat{T}_2)\|\,\|\hat{T}_1 - \hat{T}_2\| +\\ &\qquad \|\boldsymbol{u}_1 - \boldsymbol{u}_2\|\|\nabla(\hat{\alpha}_1 - \hat{\alpha}_2)\| + \|W_Z(\hat{T}_1) - W_Z(\hat{T}_2)\|\,\|\hat{\alpha}_1 - \hat{\alpha}_2\| + W_M\|\hat{\alpha}_1 - \hat{\alpha}_2\|\|\hat{T}_1 - \hat{T}_2\|.\end{aligned}$$

Applying the mean value theorem to function $W_Z(\cdot)$, Sobolev injection and the Poincaré–Friedrichs and Young's inequalities, we obtain

$$\begin{aligned}\frac{\lambda_1}{2}\|\nabla(\hat{T}_1 - \hat{T}_2)\|^2 + \frac{\gamma_1}{2}\|\nabla(\hat{\alpha}_1 - \hat{\alpha}_2)\|^2 \le \frac{M_T^2 C_S^2}{2\lambda_1}\,\|\boldsymbol{u}_1 - \boldsymbol{u}_2\|^2_{\boldsymbol{L}^3} + \frac{1}{2\gamma_1}\|\boldsymbol{u}_1 - \boldsymbol{u}_2\|^2 +\\ C_{PF}^2\left(|W'_Z(\xi_{1,T})|^2 + C_{PF}^2\frac{|W'_Z(\xi_{2,T})|^2 + W_M^2}{4\,\gamma_1}\right)\|\nabla(\hat{T}_1 - \hat{T}_2)\|^2,\end{aligned}$$

where $\xi_{i,T}$, $i = 1, 2$ are between $\hat{T}_1$ and $\hat{T}_2$. Using (36) and (44), we get

$$\begin{aligned}\lambda_1\|\nabla(\hat{T}_1 - \hat{T}_2)\|^2 + \gamma_1\|\nabla(\hat{\alpha}_1 - \hat{\alpha}_2)\|^2 \le \left(\frac{M_T^2 C_S^2}{\lambda_1\mu_1^2} + \frac{C}{\gamma_1\mu_1^2}\right)(R_p + L_\mu M'_T)^2\,\|\nabla(T_1 - T_2)\|^2 +\\ C_{PF}^2\left(2|W'_Z(\xi_{1,T})|^2 + C_{PF}^2\frac{|W'_Z(\xi_{2,T})|^2 + W_M^2}{2\,\gamma_1}\right)\|\nabla(\hat{T}_1 - \hat{T}_2)\|^2.\end{aligned} \tag{46}$$

On the other hand, the second derivative of function $W_Z(\cdot)$ is

$$W''_Z(x) = \frac{Z\,W_Z(x)}{(1 + \delta Z x)^4}\left(Z - 2\delta Z - 2\delta^2 Z^2\,x\right).$$

For $x \geq -1$, $\quad Z - 2\delta Z - 2\delta^2 Z^2\, x \leq Z - 2\delta Z + 2\delta^2 Z^2$. Thanks to (39), $W''_Z(x) \leq 0$, hence the function W'_Z is decreasing on $[-1, +\infty[$ and

$$W'_Z(\xi_{i,T}) \leq W'_Z(-1) = \frac{Z^2}{(1-\delta Z)^2}\exp\left(\frac{Z}{\delta Z - 1}\right), \qquad i = 1, 2.$$

Consequently, for Z small enough and λ_1, γ_1 and μ_1 are large enough such that hypothesis (40) hold, we deduce that

$$\|\nabla(\hat{T}_1 - \hat{T}_2)\|^2 \leq K\|\nabla(T_1 - T_2)\|^2.$$

Owing (40), we use the fixed point of Banach theorem to conclude. □

5. Analysis of the iterative scheme

For the numerical solution, we propose an efficient iterative scheme based on the Picard method to deal with the nonlinearities present in the problem (20)-(23). In the Picard iteration procedure, the Darcian velocity obtained using the temperature computed at the previous iteration, is substituted into the convective terms of the temperature and depth of conversion equations. Thus, the implementation of the proposed iterative scheme is carried out in the following steps:

1. Given an initial guess $(\boldsymbol{u}_0, p_0, \Theta_0, \Psi_0)$.
2. Until convergence:

Step 1: Given (T_k), compute the solution $(\boldsymbol{u}_{k+1}, p_{k+1}) \in \boldsymbol{L}^3(\Omega) \times (H^1(\Omega) \cap L^2_0(\Omega))$ of equation

$$\begin{aligned} \int_\Omega \mu(T_k)\boldsymbol{u}_{k+1} \cdot \boldsymbol{v}\, d\Omega + \int_\Omega \boldsymbol{v} \cdot \nabla p_{k+1}\, d\Omega &= \int_\Omega \boldsymbol{f}(T_k) \cdot \boldsymbol{v}\, d\Omega, \qquad \forall \boldsymbol{v} \in \boldsymbol{L}^2(\Omega), && (47)\\ \int_\Omega \boldsymbol{u}_{k+1} \cdot \nabla q\, d\Omega &= 0, \qquad \forall q \in H^1(\Omega) \cap L^2_0(\Omega). && (48) \end{aligned}$$

Step 2: Given the solution $\boldsymbol{u}_{k+1}$, compute $T_{k+1} \in H^1(\Omega)$ such that

$$T_{k+1}\Big|_{y=-L} = 0, \qquad T_{k+1}\Big|_{y=L} = -1,$$

and

$$\int_\Omega \boldsymbol{u}_{k+1} \cdot \nabla T_{k+1}\, \varphi\, d\Omega + \int_\Omega \lambda(\boldsymbol{x})\nabla T_{k+1} \cdot \nabla\varphi\, d\Omega = \int_\Omega W_Z(T_k)\Phi_\alpha(\alpha_k)\, \varphi\, d\Omega, \quad \forall \varphi \in H^1_{\Gamma_d}(\Omega). \quad (49)$$

Step 3: Given the solution $\boldsymbol{u}_{k+1}$, compute $\alpha_{k+1} \in H^1(\Omega)$ such that

$$\alpha_{k+1}|_{y=-L} = 1, \qquad \alpha_{k+1}|_{y=L} = 0,$$

and

$$\int_\Omega \boldsymbol{u}_{k+1} \cdot \nabla\alpha_{k+1}\, \eta\, d\Omega + \int_\Omega \gamma(\boldsymbol{x})\nabla\alpha_{k+1} \cdot \nabla\eta\, d\Omega = \int_\Omega W_Z(T_{k+1})\Phi_\alpha(\alpha_k)\, \eta\, d\Omega, \quad \forall \eta \in H^1_{\Gamma_d}(\Omega). \quad (50)$$

To establish the convergence of the proposed iterative scheme, we shall prove the following theorem:

Theorem 5.1. *Under the same assumptions as in Theorem 4.5, the iterative scheme* (47)-(50) *converges strongly in* $\boldsymbol{L}^2(\Omega) \times H^1(\Omega) \times H^1(\Omega) \times H^1(\Omega)$ *to the unique solution of problem* (20)-(23). *Furthermore, for all* $k \geq 1$,

$$\Big\|\boldsymbol{u}_{k+1} - \boldsymbol{u}_k\Big\|_{\boldsymbol{L}^3} \leq \frac{C}{\mu_1}\,(R_p + L_\mu M'_T)\,\|\nabla(T_k - T_{k-1})\|. \quad (51)$$

Proof. Taking $\boldsymbol{v} = \boldsymbol{u}_{k+1} - \boldsymbol{u}_k$ in (47) and using same techniques in the last proof, we find

$$\mu_1 \|\boldsymbol{u}_{k+1} - \boldsymbol{u}_k\| \leq C\,(L_\mu M'_T + R_p)\, \Big\|\nabla (T_k - T_{k-1})\Big\|, \qquad \forall k \geq 1, \tag{52}$$

where M'_T is defined in (41). As previously, the pair $(\mathbf{U}_k, P_k) := (\boldsymbol{u}_{k+1} - \boldsymbol{u}_k, p_{k+1} - p_k)$ is solution of the following Darcy system

$$\begin{aligned} \mathbf{U}_k + \frac{1}{\mu(T_k)} \nabla P_k &= \mathsf{F}_k := \frac{R_p}{\mu(T_k)} (T_k - T_{k-1}) \boldsymbol{e} + \frac{\mu(T_k) - \mu(T_{k-1})}{\mu(T_k)} \boldsymbol{u}_k, \\ \nabla \cdot \mathbf{U}_k &= 0. \end{aligned} \tag{53}$$

Then, we can obtain for all $k \geq 1$

$$\Big\|\boldsymbol{u}_{k+1} - \boldsymbol{u}_k\Big\|_{\boldsymbol{L}^3} \leq \frac{C}{\mu_1} (R_p + L_\mu M'_T)\, \Big\|\nabla (T_k - T_{k-1})\Big\|. \tag{54}$$

Next, by taking test functions $\varphi = T_{k+1} - T_k$ and $\eta = \alpha_{k+1} - \alpha_k$ in (49) and (50), respectively, we have

$$\begin{aligned} \lambda_1 \|\nabla (T_{k+1} - T_k)\|^2 + \gamma_1 \|\nabla (\alpha_{k+1} - \alpha_k)\|^2 \leq \left(\frac{M_T^2 C_S^2}{\lambda_1 \mu_1^2} + \frac{C}{\gamma_1 \mu_1^2} \right) (R_p + L_\mu M'_T)^2 \, \|\nabla (T_k - T_{k-1})\|^2 + \\ C_{PF}^2 \left(2|W'_Z(\xi_{1,T})|^2 + C_{PF}^2 \frac{|W'_Z(\xi_{2,T})|^2 + W_M^2}{2\,\gamma_1} \right) \|\nabla (T_{k+1} - T_k)\|^2. \end{aligned} \tag{55}$$

Hence, we conclude that for all $k \geq 1$

$$\Big\|\nabla (T_{k+1} - T_k)\Big\|^2 \leq K \Big\|\nabla (T_k - T_{k-1})\Big\|^2,$$

where $K < 1$ is defined in (40). This gives the convergence of the sequence and to finish the proof, it is easy to verify that the obtained limit satisfies problem (20)-(23), then we skip it. $\square$

6. Numerical results

To evaluate the performance of the proposed iterative scheme, we present numerical results for two examples of the coupled problem (47)-(50). In our computations, we use the quadratic $\mathbb{P}_2$ finite elements for the temperature T and depth of conversion α whereas the mixed Raviart-Thomas $RT1$ elements are used for the velocity and pressure, see [32] among others. **It should be noted that the theory of this class of mixed finite element formulations reported in [11] provides compatibility conditions on spaces to ensure the numerical stability of the coupled problem (10). Here, the considered system fits into the classical framework of perturbed saddle-point problems. Therefore, it ensures the stability conditions relevant to the considered problems, following closely the well-established Brezzi's classical treatment [11]. It is also possible to describe the inf-sup test [16], which is a numerical test widely used for checking the compatibility of specific functions spaces in the discrete formulation. In addition, as demonstrated in [10], the mixed Raviart-Thomas $RT1$ elements preserve the local mass conservation.** The numerical implementation of the considered finite element methods is carried out using the Freefem++ software [24]. Here, to solve the resulting linear systems of algebraic equations, we consider a preconditioned Generalized Minimal Residual (GMRES) iterative solver proposed in [33] with a stopping criteria set to 10^{-6}.

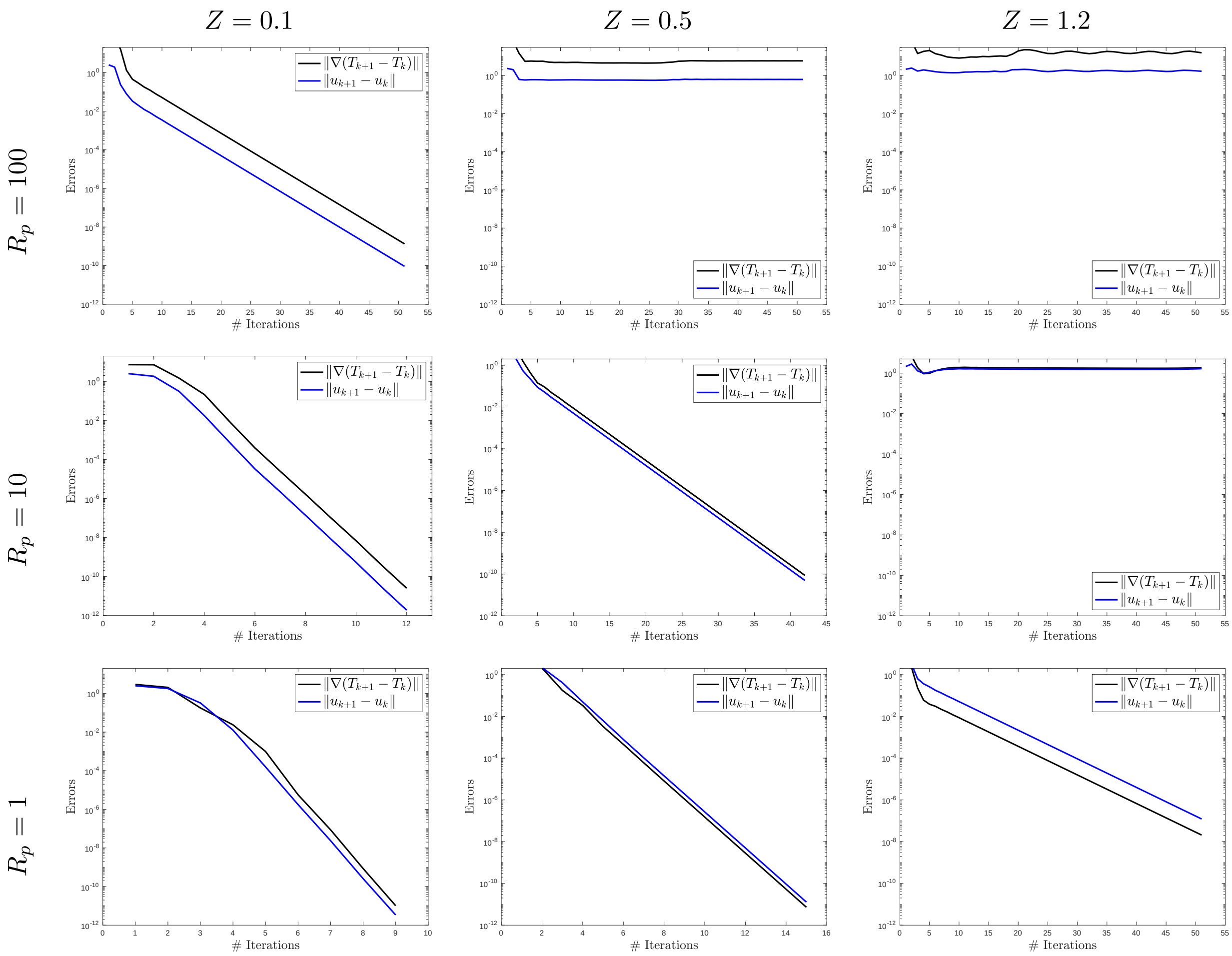

Figure 1: Convergence results obtained for the accuracy test example using $Z = 0.1$ (first column), $Z = 0.5$ (second column) and $Z = 1.2$ (third column) with $R_p = 100$ (first row), $R_p = 10$ (second row) and $R_p = 1$ (third row).

6.1. Accuracy test example

In this test example, we examine the convergence of the proposed iterative scheme (47)-(50) for solving the coupled problem (20)-(23). The computational domain is assumed to be a squared domain $\Omega = [0, 1] \times [0, 1]$. We define the functions $\mathbf{f}$ and $\mathcal{K}$ in the problem (10a)-(10b) as follows

$$\mathbf{f}(T) = R_p \left(T + T_0\right) \boldsymbol{e} + \mathbf{f}_0, \qquad \mathcal{K}(T, \alpha) = W_Z\left(T\right) \Phi_\alpha(\alpha) + \mathcal{K}_0,$$

and we choose the right-hand side functions $\mathbf{f}_0$ and $\mathcal{K}_0$ such that the problem (10a)-(10b) has an exact solution given by

$$\boldsymbol{u}(x, y) = curl\phi, \qquad p(x, y) = \cos(\pi x)\cos(\pi y),$$

$$T(x, y) = xy(x-1)(y-1)\phi(x, y), \qquad \alpha(x, y) = xy(x-1)(y-1),$$

with

$$\phi(x, y) = e^{-10\left((x-0.5)^2 + (y-0.5)^2\right)}.$$

Notice that the boundary conditions are also computed using the above exact solutions. In our numerical tests, we use the same form of fluid viscosity $\mu(T)$ defined in (12) with $\mu_\infty = 1$, $\nu = 0.5$ and $T_0 = 0$, and we fix the thermal conductivity and depth diffusivity as $\lambda = 0.1$ and $\gamma = 1$, respectively. The Rayleigh number R_p varies over the values 1, 10 and 100, and the Zeldovich number Z varies in the interval $[10^{-5}, 2]$. Taking into account Theorem 5.1, we may introduce the jth convergence rate L_j, $j = 1, \dots$ as

$$L_j := \frac{\|T_{j+1} - T_j\|_{H^1(\Omega)}}{\|T_j - T_{j-1}\|_{H^1(\Omega)}}.$$

We then, define the convergence rate L of the algorithm (47)-(50) and its mean value $\bar{L}$ as

$$L := L_J \qquad \text{and} \qquad \bar{L} := \frac{1}{J - j_0 + 1} \sum_{j=j_0}^{j=J} L_j,$$

where the indexes J and j_0 are the first iterations which, for the given tolerances, verify

$$\|T_{J+1} - T_J\|_{H^1(\Omega)} \leq 10^{-10} \qquad \text{and} \qquad \|T_{j_0+1} - T_{j_0}\|_{H^1(\Omega)} \leq 10^{-5}.$$

To illustrate effects of the change in the Rayleigh number R_p and the Zeldovich number Z, we present in Figure 1 the plots of the errors between two successive iterative solutions. In all these results, we observe that when we increase the value of the parameter Z, it leads to an increase of the numerical errors, in particular when Z exceeds a certain threshold value namely, 1 for $R_p = 1$, 0.5 for $R_p = 10$ and 0.1 for $R_p = 100$. It is also clear that the convergence of the iterative scheme is achieved for all values of the Zeldovich number satisfying $Z \leq 1$ which is expected according to Theorem 4.5. However, the numerical results show that this can only be obtained for relatively small values of the Rayleigh number R_p. For the considered test cases, we clearly notice that the error plots keep the same trend which is also consistent with the error estimates proved in the estimate (54). It should be mentioned that other numerical simulations, which are not presented here for brevity, were also performed outside this range of values for the parameters Z and R_p, and the obtained results show the same patterns.

6.2. Problem of flame propagation in a porous medium

In this test example, we use the iterative scheme (47)-(50) for solving the problem of flame propagation in a porous medium for which the mathematical governing equations are given by (20)-(23). Notice that in the context of combustion, a flame propagation refers to the process by which a flame front advances through a combustible mixture. Thus, the flame front is defined by the boundary between unburned and burned regions of the mixture and it is mainly characterized by high gradients in the temperature and conversion depth solutions. In thermal engineering, understanding dynamics of the flame propagation is important for predicting the performance and emission of combustion systems, and for developing strategies to improve combustion efficiency and reduce pollutant emissions. In this example, the computational domain is assumed to be rectangular $\Omega = [-2, 2] \times [0, 6]$ with side walls at $x = -2$ and $x = 2$ are maintained at constant cold temperature T_{cold} and conversion depth α_{cold}, see Figure 2 for an illustration. The upper wall is assumed to be adiabatic whereas, the bottom wall is divided into two parts using the inlet region $[-r_0, r_0]$ and the following boundary conditions

$$T(x, y) = \begin{cases} T_{cold} + (T_{hot} - T_{cold}) \left(1 - \dfrac{x^2}{r_0^2}\right), & \text{if} \quad x \in [-r_0, r_0], \\ T_{cold}, & \text{elsewhere,} \end{cases}$$

and

$$\alpha(x, y) = \begin{cases} \alpha_{cold} + (\alpha_{hot} - \alpha_{cold}) \left(1 - \dfrac{x^2}{r_0^2}\right), & \text{if} \quad x \in [-r_0, r_0], \\ T_{cold}, & \text{elsewhere,} \end{cases}$$

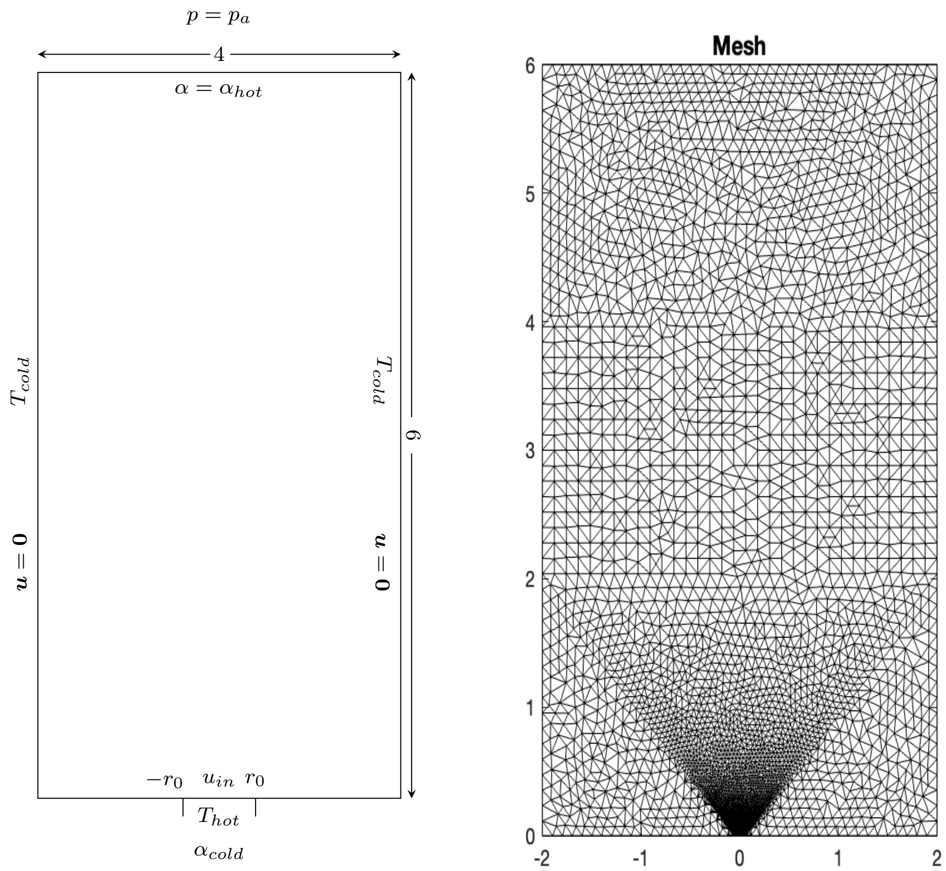

Figure 2: Illustration of the computational domain along with boundary conditions (left plot) and the unstructured mesh used in simulations for $Z = 0.1$ and $R_p = 10$ (right plot).

are used for the temperature and conversion depth solutions, respectively. Except for the bottom wall, no-slip boundary conditions are used for the velocity solution everywhere on the domain boundaries. Since the inlet velocity affects the flame features in combustion, we impose a regularized profile using the hyperbolic tangent to describe the velocity transition at the left to right ends of the inlet as

$$
v(x,y) = \begin{cases}
v_m \left(\tanh\left(\dfrac{1}{\tau}\left(1 - \dfrac{x}{r_0}\right)\right) x \right), & \text{if} \quad x \in]r_0, 2[, \\[2ex]
-v_m \left(\tanh\left(\dfrac{1}{\tau}\left(1 - \dfrac{x}{r_0}\right)\right) x \right), & \text{if} \quad x \in]0, r_0[, \\[2ex]
v_m \left(\tanh\left(\dfrac{1}{\tau}\left(1 + \dfrac{x}{r_0}\right)\right) x \right), & \text{if} \quad x \in]-r_0, 0[, \\[2ex]
-v_m \left(\tanh\left(\dfrac{1}{\tau}\left(1 + \dfrac{x}{r_0}\right)\right) x \right), & \text{if} \quad x \in]-2, -r_0[.
\end{cases}
$$

For this example, we use the following parameters $T_{cold} = -1$, $T_{hot} = 0$, $\alpha_{cold} = 0$, $\alpha_{hot} = 1$, $r_0 = 1/20$, $v_m = 1$ and $\tau = 0.02$. The thermal diffusivity coefficient is set to $\lambda = 0.1$, depth diffusivity coefficient $\gamma = 1$, the fluid viscosity is defined by (12) with $\mu_\infty = 1$, $\nu = 0.5$ and $T_0 = 0$. In order to evaluate the efficiency of the proposed iterative scheme for solving problems of front propagation in porous media, we

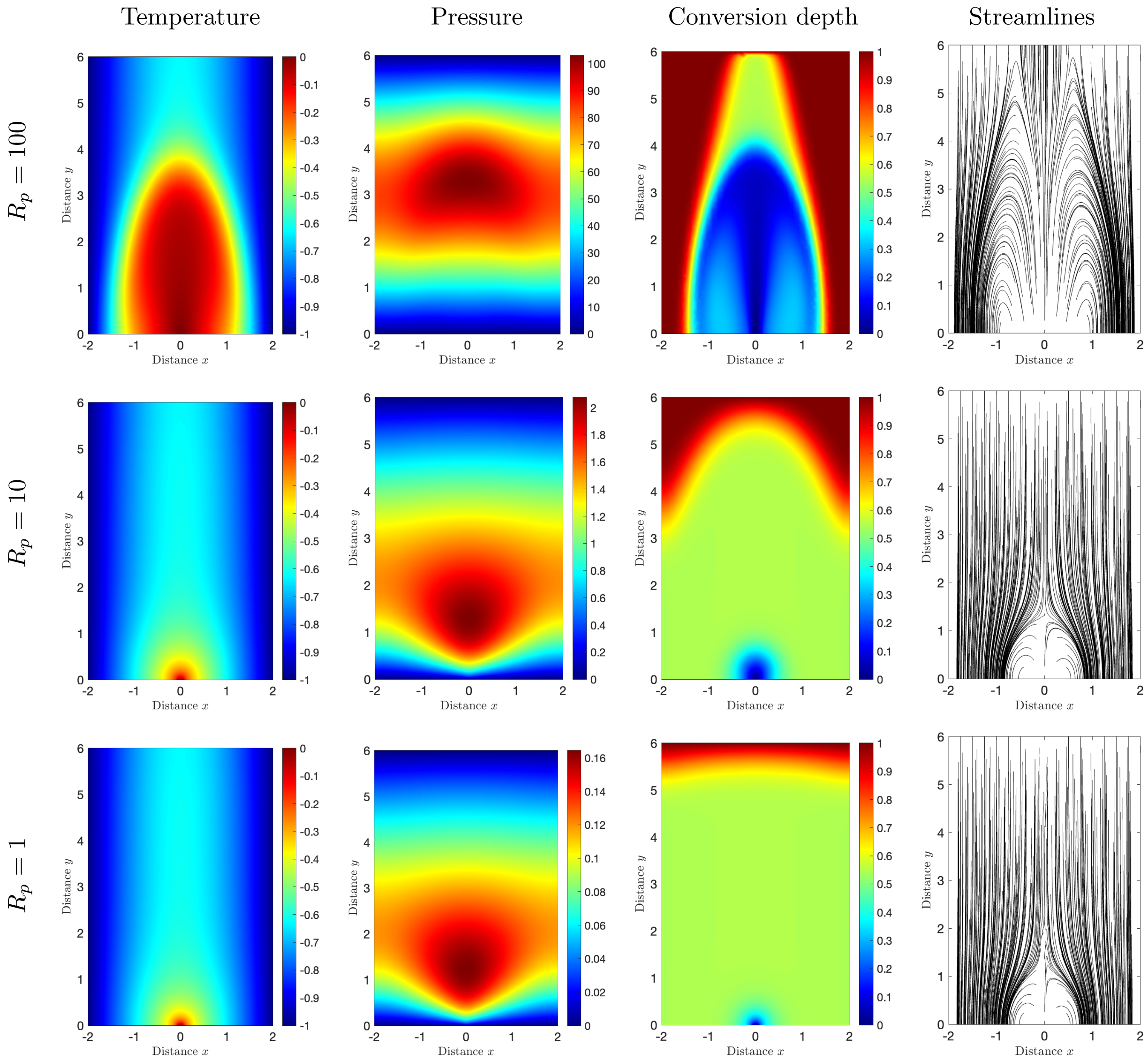

Figure 3: Results obtained for the temperature (first column), pressure (second column), conversion depth (third column) and streamlines (fourth column) with $Z = 0.1$ using $R_p = 100$ (first row), $R_p = 10$ (second row) and $R_p = 1$ (third row) for the front propagation problem.

consider three different values for the Rayleigh number namely $R_p = 1$, 10 and 100 while, the Zeldovich number is set to $Z = 0.1$ and $Z = 1$. Unstructured triangular meshes as shown in Figure 2 are used in our simulations and the associated numbers of elements and nodes are given in Table 1. Here, the selection of these meshes is based on a convergence study which is not reported here for reasons of brevity. **Note that a refined mesh is considered near the flame injection to accurately capture its propagation for the considered flow regimes. It should also be noted that the structure of the matrix system in the corresponding linear systems depends on the selection of the computational mesh but the considered solver show no difficulties in dealing with these linear systems.** In this example, the tolerance is set at $\epsilon = 10^{-7}$ such that when the variation resulting from two successive solutions is less than ϵ, the iterations are terminated. Figure 3 illustrates snapshots of the temperature, conversion depth, pressure

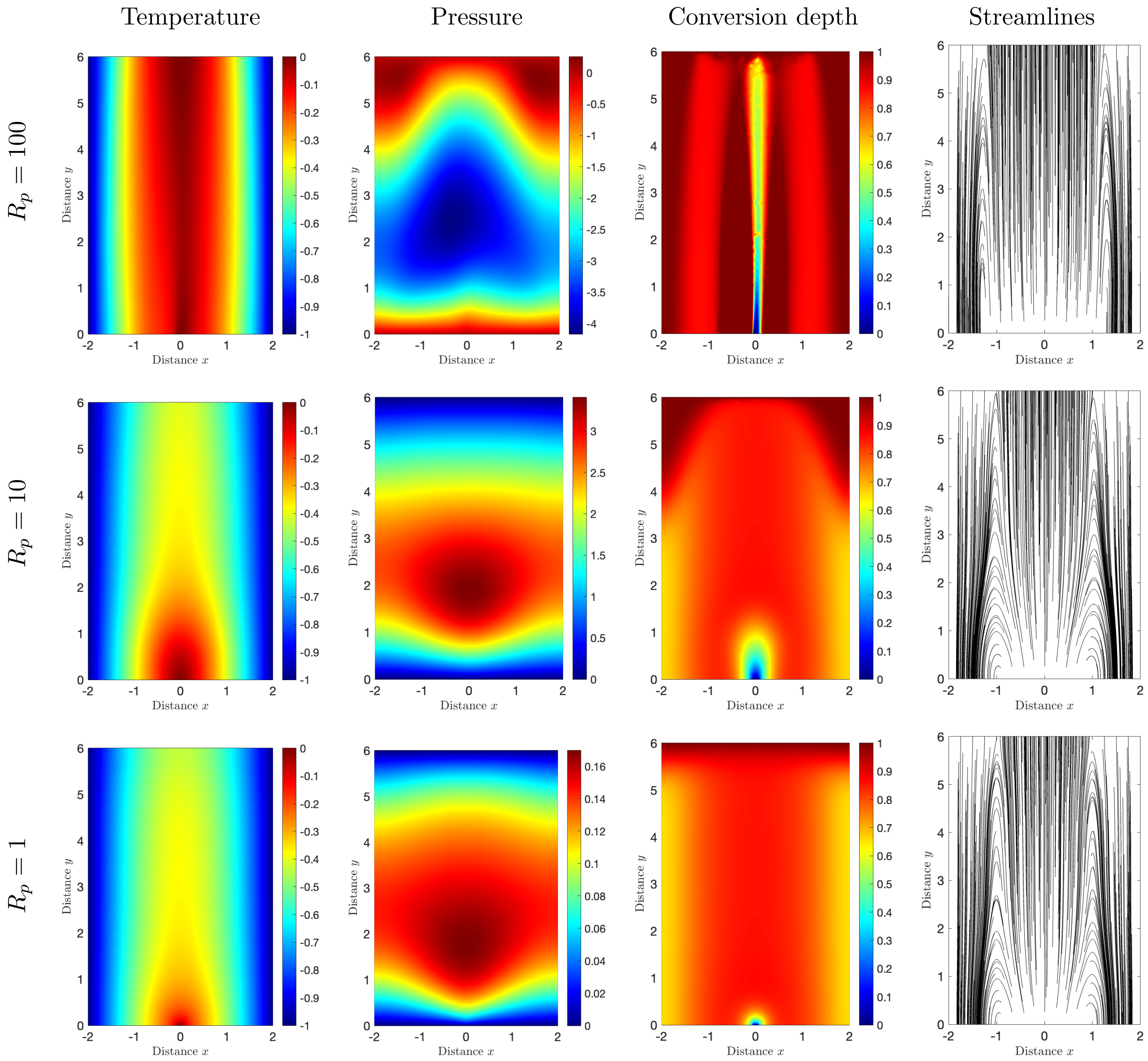

Figure 4: Results obtained for the temperature (first column), pressure (second column), conversion depth (third column) and streamlines (fourth column) with $Z = 1$ using $R_p = 1$ (first row), $R_p = 10$ (second row) and $R_p = 100$ (third row) for the front propagation problem.

and streamlines obtained at the final iteration for the considered values of the Rayleigh number R_p and Zeldovich number $Z = 0.1$. Notice that in the front propagation problems, heat is transferred through the fluid in a smooth laminar fashion for low values of the Rayleigh number. However, as the Rayleigh number increases, temperature gradients in the reaction zone become higher and convection cells with a propagating front are formed in the fluid leading to a rapid heat transfer. This also applies to the distribution of depth conversion in the fluid as shown in Figure 3 which clearly depicts the influence of the Rayleigh number on the position of the flame front and the flame propagation speed. A simple inspection of streamlines in Figure 3 reveals that, for low values of the Rayleigh number ($R_p = 1$ and $R_p = 10$) small recirculation zones near the inlet. However, for the high Rayleigh number ($R_p = 100$) the streamlines exhibit large recirculation zones near the flame inlet propagating upwards in the computational domain. In this case, the viscous effects

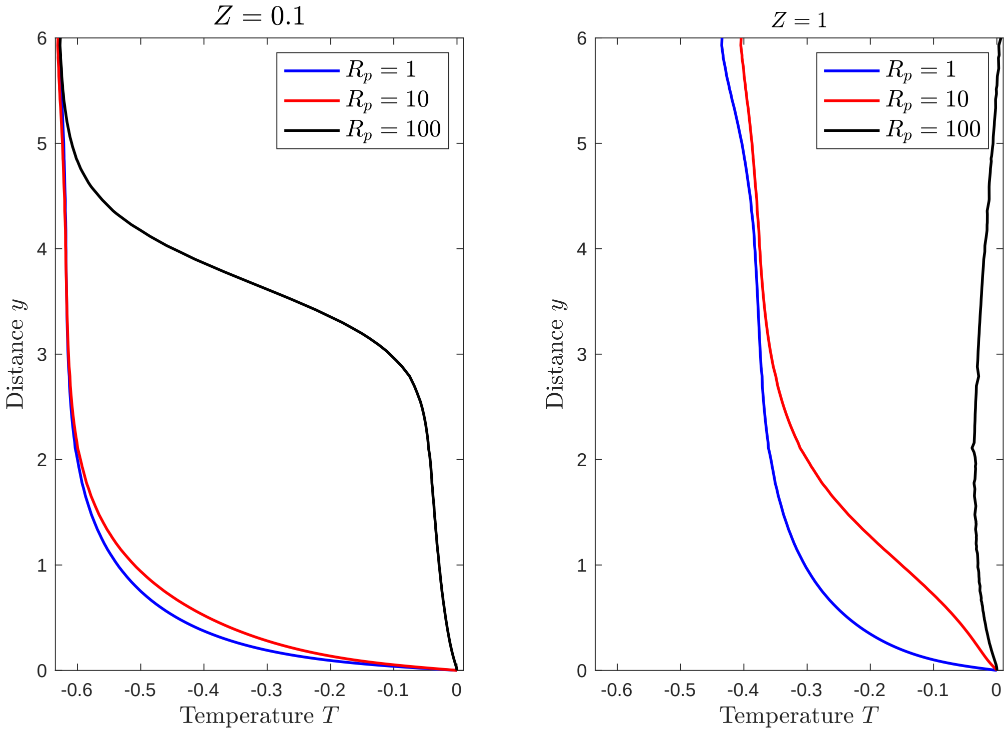

Figure 5: Vertical cross-sections of the temperature at $x = 0$ for $Z = 0.1$ (left plot) and $Z = 1$ (right plot) using different values of R_p for the front propagation problem.

become less important and the buoyancy forces become stronger such that the convection is the dominant form of heat transfer in this front propagation problem.

In Figure 4, we present results obtained for the considered values of the Rayleigh number and for a Zeldovich number set to $Z = 1$. It should be noted that the Zeldovich number is an important parameter that determines the extent to which reactants are consumed during a combustion reaction as it propagates through a fluid. In general, for low Zeldovich numbers, the reaction rate is high and the flame is expected to propagate steadily through the fluid. However, for high Zeldovich numbers, reactants diffuse rapidly away from the flame front causing it to become unstable and eventually extinguish. Therefore, controlling the Zeldovich number is important for optimizing combustion processes and ensuring stable flame propagation. The results shown in Figure 4 illustrate this effect of the Zeldovich number on the front propagation of the flame especially when compared with those results presented in Figure 3. It is clearly seen that a higher Zeldovich number quickly leads to changes in the streamlines which extend upwards from the inlet zone in the computational domain. To further illustrate these effects, we compare in Figure 5 the vertical cross-sections of the temperature at $x = 0$ using the considered values of the Rayleigh and Zeldovich numbers. It should be mentioned that for high Rayleigh and Zeldovich numbers, numerical solutions are sensitive to the mesh size, compare the mesh statistics in Table 1. Indeed, when the Rayleigh number increases, it yields a decrease in the thickness of fluid layers adjacent to the wall surface and therefore, high velocity gradients appear near the walls due to the no-slip boundary conditions. As a result, the numerical simulation for this case requires a fine mesh discretization to obtain a converged solution. In addition, it is obvious from the results listed in Table 1 that increasing the Rayleigh and Zeldovich numbers leads to an increase in the number of iterations in the iterative algorithm. In this case, finer meshes are required and therefore, more iterations are needed for convergence in the proposed iterative scheme. Finally, numbers of iterations required for the proposed iterative algorithm to converge are shown in Table 1 for the considered Rayleigh and Zeldovich numbers. It is evident that increasing the Rayleigh number leads to an increase in the number of iterations in the

Table 1: Mesh statistics and numbers of iterations in the iterative algorithm using $R_p = 1$, $R_p = 10$ and $R_p = 100$ for the considered Zeldovich numbers.

	# Elements	# Nodes	# Iterations		
			$R_p = 1$	$R_p = 10$	$R_p = 100$
$Z = 0.1$	9808	5045	9	12	51
$Z = 1$	20008	10205	33	51	67

iterative algorithm. As expected, as the Rayleigh number increases, the nonlinear dependence between the Darcy equations and the convection-diffusion-reaction equations becomes more important and the adopted fixed-point technique takes longer to converge. Moreover, by analyzing the shape of the constant K in (40) which is a sufficient condition for the convergence of the iterative scheme, we observe that when the value of R_p increases, the constant K also increases and approaches 1 which slows down the procedure. However, increasing the Zeldovich number Z while satisfying the condition (39), has little effects on the constant K appearing in (40). This is consistent with the theoretical findings demonstrated in the previous sections. **In cases with high Rayleigh and Zeldovich numbers, regularization techniques could be considered to extend the convergence analysis carried out in this study. For the numerical simulations of these cases, stabilized mixed finite element method could also be an alternative choice.**

7. Conclusions

An iterative method is presented for the numerical analysis of propagating reaction front problems in porous media satisfying an Arrhenius-type law. The governing equations consist of coupling the Darcy equations for the pressure and flow field to a set of two convection-diffusion equations for the temperature and depth of conversion with nonlinear viscosity and diffusion coefficients. Assumptions on these nonlinear coefficients and reaction terms needed for the well-posedness of the coupled model are also discussed. To prove the existence and uniqueness of weak solutions for the considered system, a fixed-point method is proposed and an iterative algorithm is used for the solution of the associated fixed-point problem. Convergence of the iterative method is also demonstrated for this class of nonlinear systems. To assess the performance of the proposed method, numerical results obtained for an example with known analytical solution and for a flame propagation problem are presented. Computational results obtained for both examples show good numerical convergence and validate the established theoretical estimates. Future work will focus on establishing error estimates for the fully discrete problems. For instance, using a mixed finite element method for the space discretization, the convergence of the iterative method could be achieved. Extension of this analysis to unsteady propagation of reaction fronts in porous media is also considered for future work.

References

[1] R.A. Adams and J. Fournier. *Sobolev Spaces*. Academic Press, 2003.

[2] F. Allali, K. Bikany, A. Taik, and V. Volpert. Numerical simulations of heat explosion with convection in porous media. *Combustion Science and Technology, Taylor & Francis*, 187:3:384–395, 2014.

[3] K. Allali, A. Ducrot, A. Taik, and V. Volpert. Convective instability of reaction fronts in porous media. *Math. Model. Nat. Phenom.*, 2(2):20–39, 2007.

[4] I. Babuška. The finite element method with lagrangian multipliers. *Numerische Mathematik*, 20(3):179–192, 1973.

[5] M. Bause and P. Knabner. Numerical simulation of contaminant biodegradation by higher order methods and adaptive time stepping. *Computing and Visualization in Science*, 7(2):61–78, 2004.

[6] A. Bejan, I. Dincer, S. Lorente, A. Miguel, and H. Reis. *Porous and complex flow structures in modern technologies*. Springer Science & Business Media, 2004.

[7] A. Bensoussan, J-L. Lions, and G. Papanicolaou. *Asymptotic analysis for periodic structures*, volume 5 of *Studies in Mathematics and its Applications*. North-Holland Publishing Co., Amsterdam-New York, 1978.

[8] J-M E. Bernard. Density results in Sobolev spaces whose elements vanish on a part of the boundary. *Chin. Ann. Math. Ser. B*, 32(6):823–846, 2011.

[9] C. Bernardi, S. Maarouf, and D. Yakoubi. Spectral discretization of Darcy's equations coupled with the heat equation. *IMA J. Numer. Anal.*, 36(3):1193–1216, 2016.

[10] C. Bernardi, Y. Maday, and F. Rapetti. *Discrétisations Variationnelles de Problèmes Aux Limites Elliptiques.* Mathématiques et Applications. Springer, Berlin, Heidelberg, 2004.

[11] D. Boffi, F. Brezzi, M. Fortin, et al. *Mixed finite element methods and applications*, volume 44. Springer, 2013.

[12] H.J. Borchardt and F. Daniels. The application of differential thermal analysis to the study of reaction kinetics. *J. Am. Chem. Soc.*, 79:41–46, 1957.

[13] H. Brezis. *Analyse Fonctionnelle : Théorie et Applications.* Collection "Mathématiques Appliquées pour la Maîtrise", Masson, 1983.

[14] T. Chacón Rebollo and R. Lewandowski. *Mathematical and numerical foundations of turbulence models and applications.* Modeling and Simulation in Science, Engineering and Technology. Birkhäuser/Springer, New York, 2014.

[15] N. Chalhoub, P. Omnes, T. Sayah, and R. El-Zahlaniyeh. Full discretization of time dependent convection-diffusion-reaction equation coupled with the Darcy system. *Calcolo*, 57:4, 2019.

[16] D. Chapelle and K.-J. Bathe. The inf-sup test. *Computers & structures*, 47(4-5):537–545, 1993.

[17] Z. Chen and R. Ewing. Mathematical analysis for reservoir models. *SIAM J. Math. Anal.*, pages 30, 431–453, 1999.

[18] T.F. Douglas, J. Russell. Numerical methods for convection dominated diffusion problems based on combining the method of characteristics with finite elements or finite differences. *SIAM J. Numer. Anal.*, 19:871–885, 1982.

[19] M. El-Amrani, L. Salhi, M. Seaid, and D. Yakoubi. An iterative scheme for solving a coupled darcy–convection–diffusion model. *Journal of Mathematical Analysis and Applications*, 517(2):126603, 2023.

[20] L.C. Evans. *Partial Differential Equations.* American Mathematical Society, 1998.

[21] X. Feng. On existence and uniqueness results for a coupled system modeling miscible displacement in porous media. *J. Math. Anal. Appl.*, pages 194, 883–910, 1995.

[22] A. Fumagalli and A. Scotti. A mathematical model for thermal single-phase flow and reactive transport in fractured porous media. *Journal of Computational Physics*, 434:110205, 2021.

[23] V. Girault and P.-A. Raviart. *Finite Element Methods for Navier-Stokes Equations, Theory and Algorithms*, volume 5 of *Springer Series in Computational Mathematics.* Springer-Verlag, Berlin, 1986.

[24] F. Hecht. New development in freefem++. *Journal of Numerical Mathematics*, 20(3-4):251–265, 2012.

[25] F.C. Lai and F.A. Kulacki. The effect of variable viscosity on convective heat transfer along a vertical surface in a saturated porous medium. *International Journal of Heat and Mass Transfer*, 33(5):1028–1031, 1990.

[26] K.J. Laidler. The development of the arrhenius equation. *J. Chem. Educ.*, 61:494–498, 1984.

[27] K.J. Laidler. Third edition. *Harper and Row*, page 42, 1987.

[28] S. Maarouf and D. Yakoubi. Analysis of backward Euler/spectral discretization for an evolutionary mass and heat transfer in porous medium. *J. Math. Anal. Appl.*, 492(1):124427, 24, 2020.

[29] T. Mohsen, K. Nader, G.P. Peterson, and Y. Shannon. Challenges and progress on the modelling of entropy generation in porous media: A review. *International Journal of Heat and Mass Transfer*, 114:31–46, 2017.

[30] D.A. Nield and A. Bejan. *Mechanics of Fluid Flow Through a Porous Medium. In: Convection in Porous Media.* Springer, New York, 2013.

[31] O. Pironneau. On the transport-diffusion algorithm and its applications to the Navier-Stokes equations. *Numer. Math.*, 38:309–332, 1982.

[32] P.-A. Raviart and J.-M. Thomas. A mixed finite element method for 2-nd order elliptic problems. In *Mathematical Aspects of Finite Element Methods: Proceedings of the Conference Held in Rome, December 10–12, 1975*, pages 292–315. Springer, 1977.

[33] Y. Saad. *Iterative Methods for Sparse Linear Systems.* SIAM, Philadelphia, 2003.

[34] L. Salhi, M. El-Amrani, and M. Seaid. A Galerkin-characteristic unified finite element method for moving thermal fronts in porous media. *Journal of Computational and Applied Mathematics*, page 113159, 2020.

[35] L. Salhi, M. El-Amrani, and M. Seaid. Analysis of a Galerkin-characteristic finite element method for convection-diffusion problems in porous media. *Advances in Pure and Applied Mathematics*, 12:96–122, 2021.

[36] L. Salhi, M. El-Amrani, and M. Seaid. A stabilized semi-Lagrangian finite element method for natural convection in Darcy flows. *Computational and Mathematical Methods*, 3(6):e1140, 2021.

[37] L. Salhi, M. Seaid, and D. Yakoubi. Well-posedness and numerical approximation of steady convection-diffusion-reaction problems in porous media. *Computers & Mathematics with Applications*, 124:129–148, 2022.

[38] L. Salhi and A. Taik. Reaction fronts in porous media, influence of Lewis number, linear stability analysis. *Int. J. Adv. Appl. Math. and Mech.*, 5(1), 1 – 13, 2017.

[39] D. Vassilev and I. Yotov. Coupling Stokes-darcy flow with transport. *SIAM Journal on Scientific Computing*, 31(5):3661-3684, 2009.

[40] J. Volker and E. Schmeyer. Finite element methods for time-dependent convection–diffusion–reaction equations with small diffusion. *Computer methods in applied mechanics and engineering*, 198(3-4):475–494, 2008.

[41] Y.B. Zeldovich, G.I. Barenblatt, V.B. Librovich, and Makhviladze G.M. *The mathematical theory of combustion and explosions.* translated from the Russian by Donald McNeill. Consultants bureau (Plenum), New York, 1985.